NAIST-IS-DD1461214

Doctoral Dissertation

A Hardware Implementation of Channel Estimation for OFDM Systems with ESPAR Antenna

Rian Ferdian

September 15, 2017

Graduate School of Information Science
Nara Institute of Science and Technology

A Doctoral Dissertation
submitted to Graduate School of Information Science,
Nara Institute of Science and Technology
in partial fulfillment of the requirements for the degree of
Doctor of ENGINEERING

Rian Ferdian

Thesis Committee:

Professor Minoru Okada	(Supervisor)
Professor Yasuhiko Nakashima	(Co-supervisor)
Associate Professor Takeshi Higashino	(Co-supervisor)
Assistant Professor Duong Quang Thang	(Co-supervisor)
Assistant Professor Yafei Hou	(Co-supervisor, Okayama University)

A Hardware Implementation of Channel Estimation for OFDM Systems with ESPAR Antenna*

Rian Ferdian

Abstract

The main objective of this dissertation is to propose a low-complexity hardware realization of the channel estimation for the orthogonal frequency-division multiplexing (OFDM) system with electronically steerable parasitic array radiator (ESPAR) antenna. Consisting of a single active element surrounded by multiple parasitic elements, ESPAR antenna can achieve the similar diversity order to that of multiple antennas but only using one RF front-end hardware set. Therefore, ESPAR based system has huge potential to realize a low-cost and high energy efficiency for multiple antennas and massive antennas systems. The main drawback of the ESPAR based system is that the channel estimation usually should be realized in time-domain because the received signal for each antenna element or parasitic element will be overlapped each other both in the frequency and time domain. Therefore, among the existing methods, compressed sensing (CS) technique has been theoretically proven to be a suitable channel estimation for ESPAR antenna. However, due to its very large sensing matrix, the CS algorithm suffers from a computational burden, making it infeasible for many practical applications.

This dissertation proposes three methods to reduce the computational cost of CS in ESPAR antenna deployment. The first method is a multi-column CS which utilizes only one small segment of sensing matrix to detect all of the channel impulse response locations simultaneously. The second method is the matrix

*Doctoral Dissertation, Graduate School of Information Science,
Nara Institute of Science and Technology, NAIST-IS-DD1461214, September 15, 2017.

strength reduction by taking advantage of the sensing matrix structure which based on symmetrical properties of discrete Fourier transform (DFT) matrix. The third method is the observation vector optimization by randomly selecting small set of optimal observation vector locations at the receiver side, which can reduce the CS computation complexity involved in channel impulse response (CIR) locations search. The combination of these three methods can achieve more than 97% reduction in the computational cost. Furthermore, a parallel hardware architecture and its field programmable gate array (FPGA) implementation for the proposed channel estimation are also presented. The hardware implementation timing result can meet the real-time requirement for any wireless communication standard.

Keywords:

Channel Estimation, Compressed Sensing, Orthogonal Matching Pursuit, Matrix Strength Reduction, OFDM, DFT Matrix, Genetic Algorithm, VLSI Architecture, Field Programmable Gate Array, Computational Complexity Reduction.

Acknowledgments

First of all, I thank God for His grace and bless that allow me to achieve one of the important goals in my life on getting this Doctoral degree. I would like to express my gratitude for Professor Minoru Okada who recognized my dream three years ago and make it possible for me to study in NAIST, although I had only very limited knowledge in the communication system area. His valuable guidances and supports enable me to achieve an important result in my research. I sincerely thank my mentor, Assistant Professor Yafei Hou for his never ending encouragements and supports. Without his help, I will not be able to finish this dissertation. It was a great pleasure and honor to be working under his guidance. To my thesis committee, I would like to thank Professor Yasuhiko Nakashima for his comments and discussions during the presentation that can drive my research into a better and new direction. I also thank Associate Professor Takeshi Higashino and Assistant Professor Duong Quang Thang for the fruitful discussions and valuable inputs and advices. I would like to thank The Ministry of Education, Culture, Sports, Science and Technology in Japan (MEXT) for the financial support which allows me to pursue my Doctoral degree in NAIST. Special thank for our laboratory secretary Hayashi-san and Kioi-san, for their helps in many administration works. I also very thankful to all of my friends from Network Systems laboratory, Indonesia students group, and NAIST Moslem community. Thank you for the good friendship and give me a valuable experience during my stay in Japan. Finally, my greatest gratitude for my family, my parents, my wife, and my daughter. Thank you for your endless love and patient which give me strength every day.

Publications

Journal Articles

1. Rian Ferdian, Yafei Hou and Minoru Okada, "A Low-Complexity Hardware Implementation of Compressed Sensing-Based Channel Estimation for ISDB-T System," in *IEEE Transactions on Broadcasting*, pp. 92-102, March 2017.

International Conferences (Peer Review)

1. Rian Ferdian, Yafei Hou and Minoru Okada, "Effective VLSI architecture for compressed sensing based channel estimation in ISDB-T system," in *2015 15th International Symposium on Communications and Information Technologies (ISCIT 2015)*, pp. 273-276, Nara, Japan, October 2015.

2. Rian Ferdian, Yafei Hou and Minoru Okada, "Fast and low-complexity orthogonal matching pursuit based channel estimation in ISDB-T receiver with 3-element ESPAR antenna," in *2016 IEEE International Symposium on Broadband Multimedia Systems and Broadcasting (BMSB)*, Nara, Japan, June 2016.

Domestic Conferences (Non Peer Review)

1. Rian Ferdian, Yafei Hou and Minoru Okada, "Compressed Sensing Based Channel Estimation in ISDB-T System without Cyclic Prefix ," in *ITE Technical report 2016*, pp. 29-32, Otaru, Japan, February 2016.

2. Rian Ferdian, Ratih Hikmah Puspita, Yafei Hou and Minoru Okada, "Low Complexity Compressed Sensing Based Channel Estimation with Measurement Matrix Optimization for OFDM System," in *IEICE Technical Report 2016*, Kyoto, Japan, November 2016.

Contents

List of Figures

1 Introduction

1.1 Background

Wireless communication has been a foundation of the recent technologies advancement that transformed our world today. The demand of higher data rate services not only for getting faster mobile browsing time or higher quality television broadcasting images, but it also opens up many new technology possibilities. From social media, smartphone, cloud computing, and the internet-of-things (IoT) are growing from the benefit of high-speed data communication that can be accessed from anywhere we want.

High data-rate leads to a wide bandwidth transmission known as the broadband system. One of the challenge in the broadband system is the multi-path fading channel. In wireless communication, the transmitted signal will be propagated in many paths before it reached the receiver side, where each path has a different attenuation and delay profile. Because of the transmission time is very short in the broadband system, a signal from the previous time slot can interfere the current signal reception. At the frequency domain, the multi-path fading can be categorized into frequency-selective fading and flat-fading. The frequency-selective fading is when each frequency in the signal bandwidth has a different level of attenuation, while in the flat-fading, all the frequency in the signal bandwidth is having an almost the same attenuation. Both frequency-selective fading and flat-fading can greatly corrupt the received signal in broadband transmission.

To mitigate the multi-path fading problem, a multi-carrier technique with frequency division multiplexing (FDM) was proposed [2]. FDM divides a high-rate data stream into several low-rate data streams where each stream is transmitted with different carrier frequency [3]. The low-rate data streams are having a narrow bandwidth which robust to frequency selective fading. However, each

sub-carrier in the FDM system need a guard space to avoid inter-carrier interference, so there will be some unused frequency spectrum in this system. Moreover, the requirement for separate modulator for each sub-carrier greatly increase the system complexity.

Orthogonal frequency-division multiplexing (OFDM) is an upgrade from FDM system [4, 5]. OFDM technique features the orthogonality for each of its sub-carrier. Each orthogonal sub-carrier is having a non-interfering frequency spectrum, thus it can be placed overlapping to each other without having an interference to achieve a better efficiency in system total bandwidth. The orthogonality in the OFDM system is obtained by utilizing the inverse discrete Fourier transform (DFT) matrix as the modulator [6]. Moreover, OFDM is robust from inter-symbol interference (ISI) and easy to equalize due to its cyclic prefix (CP) [7]. OFDM has been a core of the modern wireless communication, it has been implemented in many standard such as wireless LAN [8], the cellular network [9], and digital television [10]. However, flat-fading still become a problem in the OFDM system.

Recently, multi-antenna technique, multiple-input, multiple-output (MIMO) is becoming a hot topic in the wireless communication system area. MIMO can take advantage of the spatial multiplexing or spatial diversity in the multi-antenna system. Using the spatial multiplexing where each antenna transmits a different information signal , MIMO can greatly improve the system capacity. MIMO also can take advantage of spatial, when transmitting the same signal into multiple antennas, a MIMO receiver can increae the system reliability by combining all the received signal together to improve its quality. The implementation of MIMO into OFDM system is an effective technique to fight flat-fading problem [11, 12].

Here, the electronically steerable parasitic array radiator (ESPAR) antenna offers a new method to gain diversity from multiple antennas while keeping only one RF front-end [13, 14]. ESPAR antenna is an adaptive beamforming multi-antenna system [15–18]. An ESPAR antenna consists of one radiator element and several parasitic elements. The wireless channel at each antenna's element is considered to be independent of each other. To gain diversity, ESPAR antenna changes the directivity of its input signal using inexpensive variable reactances circuits which connected to each parasitic elements. Then, all the input signals with different directivity are mixed together into one RF front-end. Hence, the

implementation of ESPAR antenna can lead to a low-power and low-cost system with the same reliability and capacity compared to MIMO systems. There have been several proposals for the implementation of ESPAR antenna into current generation of wireless communication systems which based on OFDM modulation [19,20]. However, the trade-off of this method is the complexity increment in both of equalization and channel estimation process.

The multi-path fading channel can be modeled as a Toeplitz matrix at the time domain [21]. In the conventional OFDM system, the CP addition at the transmitter and its removal at the receiver will cause the receiver to consider the multi-path fading channel as a cyclic Toeplitz matrix. The cyclic Toeplitz matrix is a special matrix as it has a diagonal structure in the frequency domain. Because of that, after the DFT process at the OFDM receiver, the channel impact can be modeled as a simple diagonal matrix multiplication. Because of its diagonal structure, the receiver can estimate the channel using several known pilot tones. Where the other part of the channel information can be recovered using interpolation method. However, in the OFDM system using ESPAR antenna, the change on directivity in the ESPAR antenna will correspond to the signal frequency shift at the frequency domain. In results, the equivalent channel for the OFDM transmission cannot be modeled as a diagonal matrix anymore. The received pilot tones at the receiver will be a combination of each element channel state. Because of that, an interpolation of the adjacent pilot tones cannot be used to get the channel profile in the ESPAR-OFDM system. This dissertation focuses on the implementation of the channel estimation for ESPAR-OFDM system.

1.2 Overview of the Problem

Compressed sensing (CS) has been proposed to solve the channel estimation problem in the ESPAR-OFDM system [20, 22–24]. CS is a new data acquisition technique that enables the reconstruction of a sparse signal with sub-Nyquist samples [25], [26]. Theoretically, the CS algorithm can recover the channel impulse response from the ESPAR-OFDM system. However, the cost of computation for the CS based channel estimation still suffer from a huge matrix inner product operation. Because of its complexity, there were also only a few schemes for CS

Table 1.1: Cyclic Prefix Duration of OFDM-based Wireless Communication Systems

Communication Standard	OFDM Symbol Duration
ISDB-T	31 μS
DVB-T2	28 μS
LTE	14 μS
Wimax	12 μS

hardware realization. Several proposals focused on reducing the least-squares complexity using modified Grahm-Schmidt [27], [28] and Cholesky decomposition [29], [30]. Since most of the realizations are based on real number, some methods such as Cholesky decomposition are not applicable for complex number problems. Moreover more than 80% of the CS computation lies on the measurement matrix multiplication as mentioned in reference [27]. The implementation of CS algorithm in a specific application can utilize several optimizations to reduce its complexity. Recently reference [31] has proposed an CS hardware realization for radar application with an improvement in inner product computation by utilizing a zero padding FFT. However, for the application where the measurement matrix is truncated in both column and row directions, the inner product using FFT method may not yield to the best reduction for its cost of computation.

Wireless communication is one of the real-time system where its computation need to be performed within a specific timing deadline. To achieve the real-time processing time, the channel estimation need to be done less than the cylic prefix duration (CP) [32]. Table 1.1 shows the CP duration for several wireless communication systems which varies from 12-31 μS. Within the symbol duration time, a receiver need to performed all the demodulation process from the channel estimation to the bit demapper. While the fastest available CS hardware implementation was presented in [31] with 158.7 μS processing time. It can be seen that the available proposals of the CS hardware implementation can not met the timing specification from Table 1.1.

1.3 Research Contributions

The execution of this dissertation is divided into two parts. To simplify the problem, at the first part, a conventional SISO (single-input, single-output) OFDM is considered as the system model. Several improvements for OFDM CS based channel estimation as below:

- CS based channel estimation in the OFDM system has a unique structure of sensing matrix which based on digital Fourier transform (DFT) matrix. Computational complexity reduction can be achieved by exploiting the periodicity and symmetry property which the measurement matrix inherits from DFT matrix to achieve lower complexity in the measurement matrix inner product computation [33, 34].

- The sensing matrix size depends on the number of pilot tones, while most of the OFDM system already designed for interpolation based channel estimation. A observation vector selection method using genetic algorithm (GA) at the receiver side is proposed to involve minimum as possible of pilot tones in the CS algorithm [35].

The second part of this dissertation is to apply the proposed OFDM CS based channel estimation into ESPAR-OFDM system. The contributions is desribed as below:

- In this transmission, each antenna element is close to each other, thus we can assume that all the CIR have the same delay profile. A multi-column OMP technique is proposed by introducing a new sensing matrix for the inner product calculation, which size is only equal to the one segment sensing matrix. Moreover, the new sensing matrix is based on DFT matrix, thus the proposed OFDM CS based channel estimation can be applied [24].

- A hardware architecture and its realization in field programmable gate array (FPGA) is also proposed to assess the effectiveness of the proposed computational reduction methods [34].

- The random access memory (RAM) usage in the hardware design can be optimized by exploiting the DFT property [34].

1.4 Outline of Dissertation

The rest of the dissertation is organized as follows. Chapter 2 presents the basic of this dissertation environment, the multi-path fading channel characteristic, OFDM system structure, MIMO system structure and ESPAR antenna. Chapter 3 introduces the channel estimation in the OFDM system with ESPAR antenna. The comparison with the conventional OFDM channel estimation and the current development of the channel estimation are presented in this chapter. This chapter also shows the computational complexity problem in the channel estimation for ESPAR-OFDM system. Chapter 4 presents the three methods for the CS computational cost reduction, multi-column OMP, matrix strength reduction and the observation vector optimization. Chapter 5 provides the VLSI implementation for the proposed method and its synthesis and timing analysis. Finally, Chapter 6 gives the conclusions of this dissertation.

2 OFDM Systems with ESPAR Antenna

This chapter presents the basic environment of this dissertation's research. The chapter 2.1 presents the knowledge of the multi-path fading in the wireless communication system. The chapter 2.2 is an overview of the standard OFDM system, its transceiver structure and its properties. Then section 2.3 gives an explanation about MIMO system and how it can improve the OFDM system performance. The last section 2.4 explains the ESPAR antenna as an improvemet to the MIMO system.

2.1 Multipath Fading Channel

A transmitted wireless signal will be propagated in many paths before it can reach the receiver side as shown in the Fig. 2.1. Basically, there are three kinds of the propagation phenomenon [36]:

- **Reflection**: When a radio signal collides with a medium which has larger surface compare to the signal 's wavelength, some of the signal property will be reflected and some is still transmitted.
- **Diffraction**: When a radio signal bounces into a sharp surface material and create a new wave.
- **Diffraction**: When a radio signal falls into a rough surface material, it will create multiple reflections.

The received signal from each path will have a different delay and attenuation. Each of these received signals will interfere each other at the receiver side. In

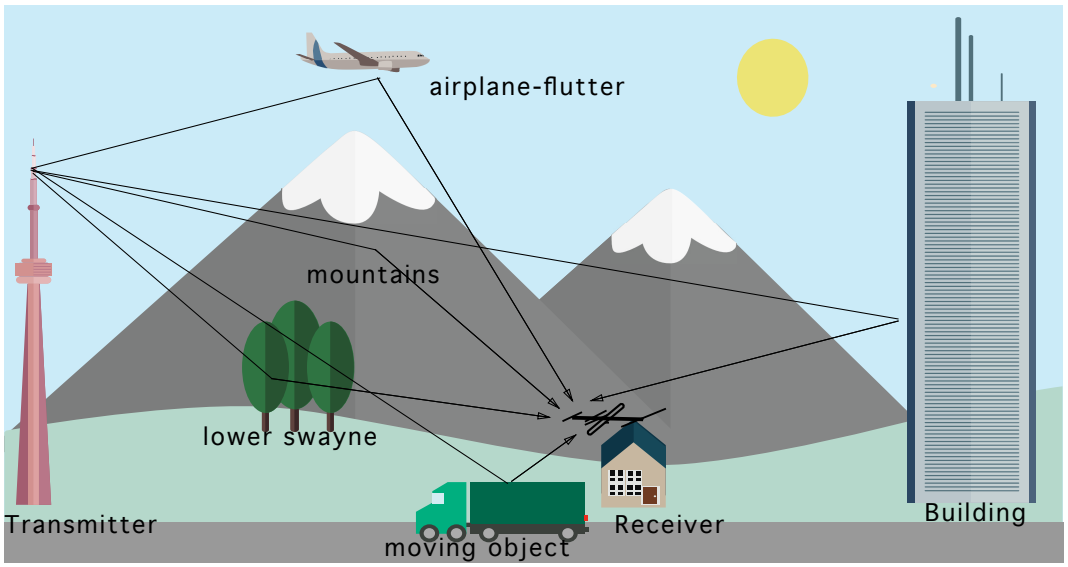

Figure 2.1: Multipath fading channel.

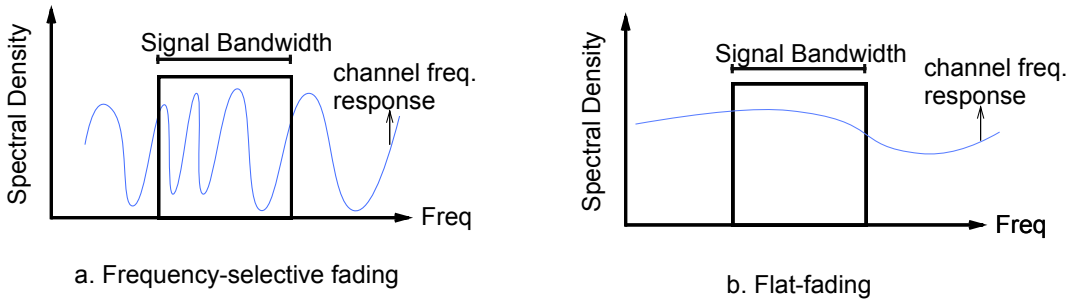

Figure 2.2: Frequency-selective fading and flat-fading.

order to reverse the channel fading effect, a receiver needs to have a channel estimation and equalization.

The multi-path fading channel also can be defined as a combination of selective-fading and flat-fading channel. The selective-fading channel is when the channel frequency response bandwidth less than signal transmission bandwidth. Here each sub-carrier can have a different level of attenuation. While, the flat-fading is the opposite when the channel frequency response bandwidth is bigger than the signal transmission. In flat-fading all the signal sub-carrier are having almost the same level of attenuation. Fig 2.2 shows the difference between frequency-

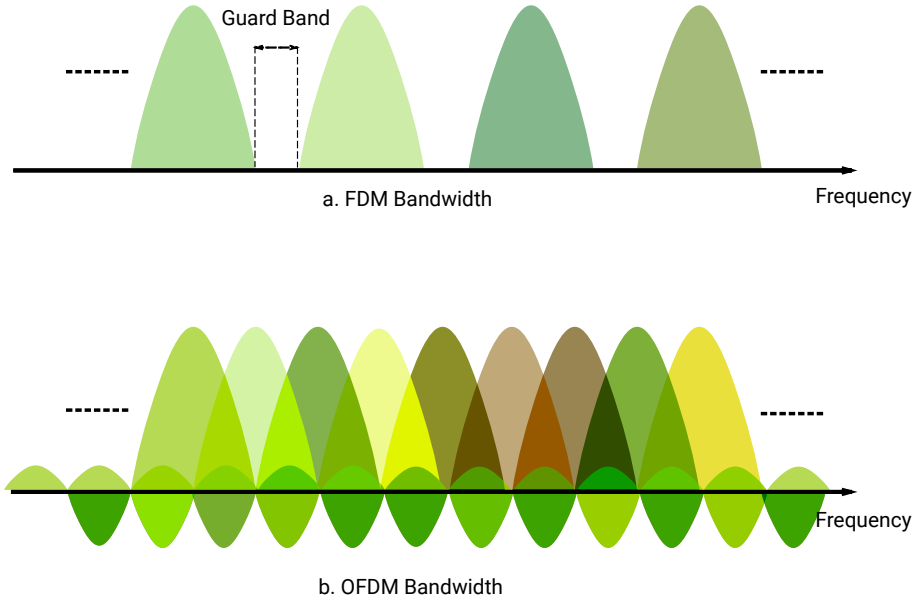

Figure 2.3: a. FDM frequency spectrum b. OFDM frequency spectrum.

selective fading and flat-fading.

2.2 OFDM System

Orthogonal frequency-division multiplexing (OFDM) is a multi-carrier modulation system. OFDM has been long proposed back in the 1970s as a frequency-division multiplexing system using the discrete Fourier transform (DFT) [37]. OFDM transform the high-rate stream of data into several low-rate streams of data and transmit it using multiple carrier of frequencies. Furthermore, each of its carriers is orthogonal to each other, as shown in the the Fig. 2.3b. It can be seen that a spectrum peak of a sub-carrier always collide with zero-crossing of other sub-carriers. Because of that as long as the data sampling can be done correctly at each sub-carriers peak, each sub-carrier can be spaced closer to each other without having an inter-carrier interference. The orthogonality of OFDM carrier is achieved by exploiting the discrete Fourier transform property. However, there was no realization of OFDM into the commercial market until the invention of fast Fourier transform (FFT). The history of OFDM is a conclusive

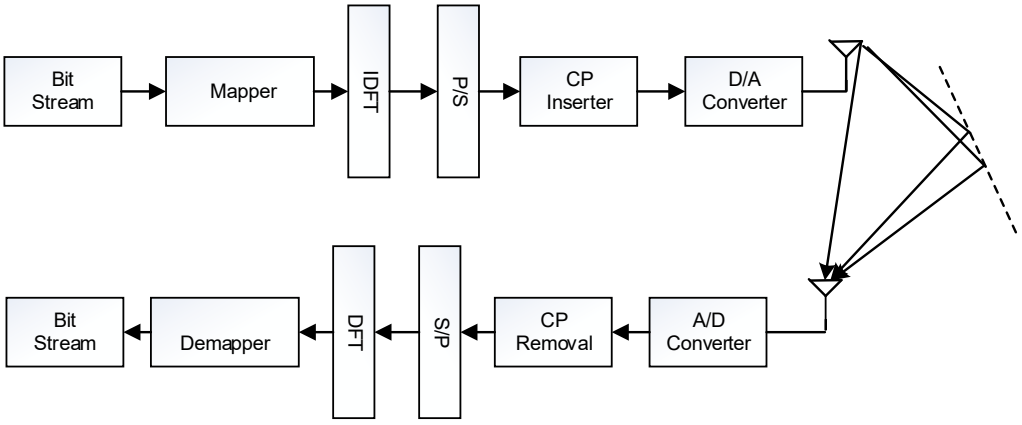

Figure 2.4: Block diagram of simplified OFDM system.

evidence of how computational complexity can hinder the implementation of a new technology.

Compare to the FDM system spectrum as shown in the Fig. 2.3a, it can be seen that, for the same bandwidth the OFDM system can accommodate more sub-carrier and achieve higher data rate compared to the FDM system. Each sub-carrier in the FDM system must have a guard band to prevent the inter-carrier interference (ICI). While in the OFDM system, because of the orthogonality of the DFT matrix the ICI can be avoided. The OFDM system only needs guard band for each symbol to prevent inter-symbol interference (ISI) from previously transmitted symbol due to the channel fading effect.

Fig.2.4 shows the structure of the simplified OFDM block diagram. To create the transmission signal, first the mapper maps the bit stream. Next, the IDFT processor will create an OFDM symbol by transforming the data sequence into the time domain. To prevent ISI, the cyclic prefix (CP) is inserted in the OFDM symbol by copying certain part of the symbol's rear to its front. Then, the transmit signal will be sent over a multipath channel. At the receiver, before the demodulation process can be done, a channel estimation and equalization are required to combat the multipath channel effects.

The time domain structure of the frequency-selective fading channel in OFDM

system can be modeled as a Toeplitz matrix $\mathbf{h} \in \mathbb{C}^{(S+L-1)\times S}$ as

$$\mathbf{h} = \begin{bmatrix} h_0 & & & 0 \\ \vdots & h_0 & & \\ h_{L-1} & \vdots & \ddots & \\ & h_{L-1} & \vdots & h_0 \\ & & \ddots & \vdots \\ 0 & & & h_{L-1} \end{bmatrix}, \tag{2.1}$$

where L is the number of CP and S is the number of OFDM sub-carriers. Here, we assume channel has L paths which includes many zero elements for easy analysis.

Another function of CP beside ISI prevention is to ease the equalization and channel estimation computation. As the receiver removes the CP from the received signal, the equivalent channel $\mathbf{h}_{eq} \in \mathbb{C}^{S\times S}$ can be treated as a circulant Toeplitz matrix given by

$$\mathbf{h}_{eq} = \begin{bmatrix} h_0 & 0 & \cdots & 0 & h_{L-1} & \cdots & h_1 \\ h_1 & \ddots & \ddots & \vdots & 0 & \ddots & \vdots \\ \vdots & \ddots & h_0 & 0 & \vdots & \ddots & h_{L-1} \\ h_{L-1} & & h_1 & \ddots & 0 & & 0 \\ 0 & \ddots & \vdots & \ddots & \ddots & \ddots & \vdots \\ \vdots & \ddots & h_{L-1} & & \ddots & \ddots & 0 \\ 0 & \dots & 0 & h_{L-1} & \cdots & h_1 & h_0 \end{bmatrix}, \tag{2.2}$$

where S is the number of OFDM subcarriers without CP. Because of the Toeplitz structure, by only knowing the channel impulse response (CIR) which defined as the first column of the $\mathbf{h}_eq$, the whole channel matrix can be reconstructed. Here CIR is $[h_0, h_1, ..., h_{L-1}, 0, ..., 0]^T$ vector.

The matrix $\mathbf{h}_{eq}$ has an advantage that its frequency domain form $\mathbf{H}$ is a diagonal matrix. Let $\mathbf{H}$ is defined as

$$\mathbf{H} = \mathbf{F}\mathbf{h}_{eq}\mathbf{F}^H, \tag{2.3}$$

where $\mathbf{F} \in \mathbb{C}^{S\times S}$ is the DFT matrix, and its hermitian $\mathbf{F}^H \in \mathbb{C}^{S\times S}$ is the IDFT

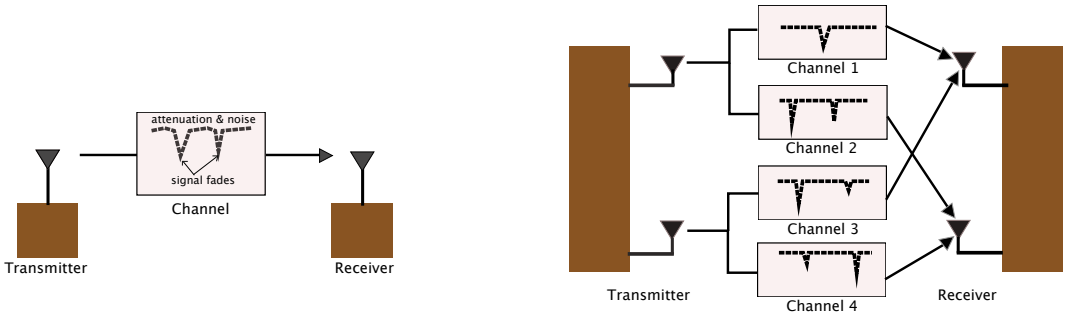

a. SISO System

b. SISO System

Figure 2.5: Comparison between SISO system and MIMO system.

matrix. The structure of matrix $\mathbf{H} \in \mathbb{C}^{S \times S}$ is represented as

$$\mathbf{H} = \begin{bmatrix} H_0 & & & 0 \\ & H_1 & & \\ & & \ddots & \\ 0 & & & H_{S-1} \end{bmatrix}, \tag{2.4}$$

where H_i is the frequency domain frequency-selective fading CSI for i-th subcarrier. Accordingly the received signal can be described as

$$\mathbf{Y} = \mathbf{HX} + \mathbf{W}, \tag{2.5}$$

where $\mathbf{W}$ is the receiver's noise $\mathbf{w}$ in the frequency domain. Thus, to equalize $\mathbf{X}$ from $\mathbf{Y}$, it only requires a simple diagonal $\mathbf{H}$ matrix inversion [38]. The frequency domain channel state information (CSI) also can be considered as the diagonal part values of the matrix $\mathbf{H}$ as $[H_0, H_1, ..., H_{S-1}]$ vector.

2.3 MIMO System

Although robust from frequency-selective fading, OFDM system is still suffered from the flat-fading problem. One effective way to fight flat-fading effect is by using multiple-input, multiple-output (MIMO) technique [11, 39, 40]. MIMO is a multi-antenna system as shown in the Fig. 2.5. Compare to the single-input, single-output (SISO) system, MIMO system has a chance to gain spatial diversity transmitting its signal into multiple different channels. At the receiver, the

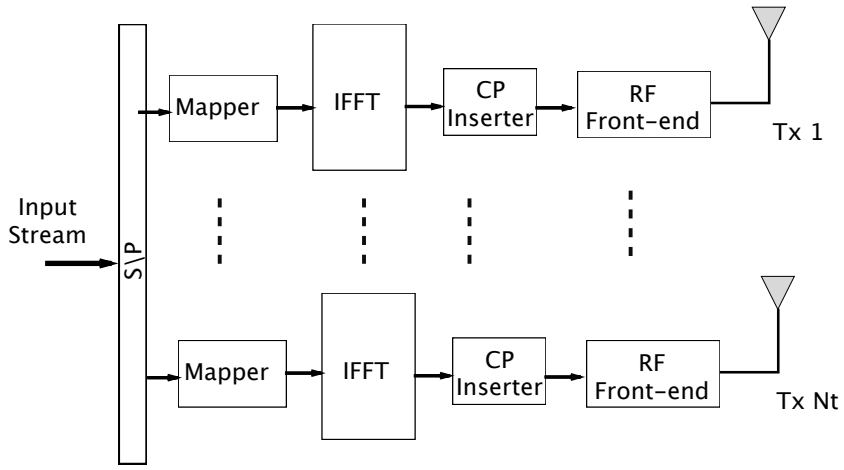

a. MIMO-OFDM Transmitter

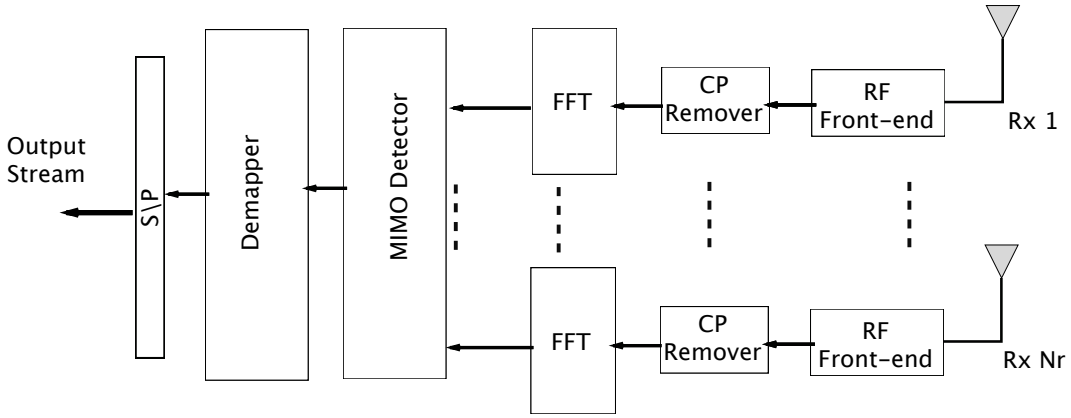

b. MIMO-OFDM Receiver

Figure 2.6: The structure of MIMO-OFDM transceiver.

received signals from each antennas are combined together to obtain a better quality signal.

For MIMO system with N_t antennas at the transmitter and N_r antennas at the receiver side, the received signal can be described as below

$$\begin{bmatrix} y_1 \\ \vdots \\ y_{N_r} \end{bmatrix} = \begin{bmatrix} h_{11} & \dots & h_{1N_t} \\ \vdots & \ddots & \vdots \\ h_{N_r1} & \dots & h_{N_rN_t} \end{bmatrix} \begin{bmatrix} x_1 \\ \vdots \\ x_{N_t} \end{bmatrix} + \begin{bmatrix} n_1 \\ \vdots \\ n_{N_r} \end{bmatrix}, \tag{2.6}$$

where $[y_1 \dots y_{N_r}]^T$ is the received signals vector, $[x_1 \dots x_{N_t}]^T$ is the transmit signal vector and $[n_1 \dots x_{N_r}]^T$ is the noise vector from each transmission channel. The application of MIMO into OFDM system can minimize the effect of the flat-fading. The structure of the MIMO-OFDM system is shown in the Fig. 2.6.

The main drawback of the MIMO is the requirement of a set radio frequency (RF) front-end devices such as A/D transfer and power amplifier which consumes over half of energy at each of antenna unit [41,42]. The large energy consumption of multiple RF front-ends refrains the usage of MIMO with large number antennas into mobile devices. On the other hand, for massive MIMO system which is one of key technique to realize target of 5G system, large number of antenna branch will not only increase power consumption and CO2 emission, but also increase the temperature of system devices which require large air-conditioners to make it work properly [43].

2.4 ESPAR Antenna

Electronically steerable parasitic array radiator (ESPAR) antenna is a novel low-cost technique to gain horizontal diversity while maintaining one RF front-end, low power consumption, and simple wiring at the mobile receiver. The structure of the ESPAR antenna hardware is shown in Fig. 2.7 a. This antenna consists of a circular ground planar as a base, one radiator element and multiple of parasitic elements. The radiator element is placed in the middle of the ground planar and connected to an active reactor. While the parasitic elements are placed surround the radiator element with the same distance and connected to a passive variable reactor diode. ESPAR antenna has been proposed to be used in very broad of

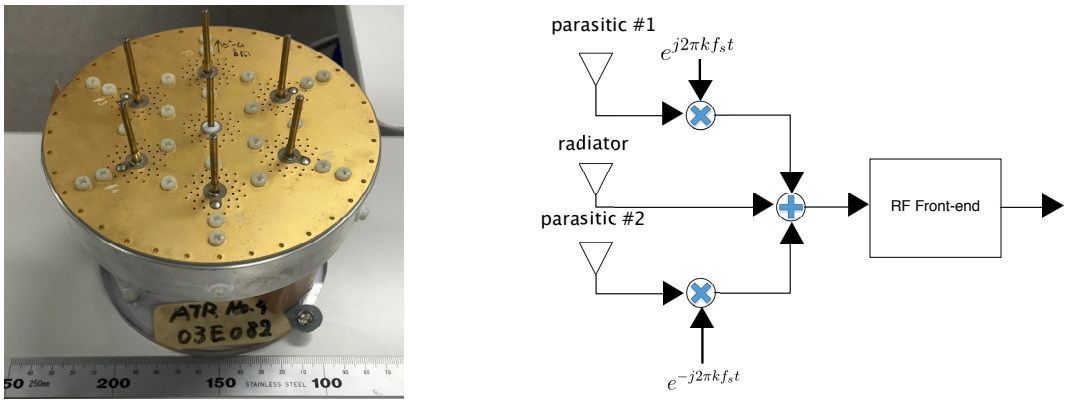

Figure 2.7: a) ESPAR antenna hardware structure, b) Equivalent circuit model for ESPAR antenna.

applications, the OFDM based wireless communication [44–46], digital broadcasting system [23, 47], truck to truck communication [48], IoT system [49], wearable system [50] and robot tracking system [51, 52]. ESPAR antenna is promising a better energy efficiency in the multi-antenna system. Wireless system using ESPAR antenna can obtain almost the similar diversity order to that of MIMO system while just using only one set of device for RF front-end [13, 14].

The beamforming is done at the analog part of the ESPAR antenna. The reactance circuit between the parasitic and the radiator element is worked as an oscillator circuit. The antenna element location, variable reactance value and the bias voltage will determine the alternating current which flow from parasitic element to the radiator element. The equivalent circuit model of the ESPAR antenna is shown in Fig. 2.7 b. The output from the antenna RF front-end can be described as

$$v(t) = v_0(t) + v_1(t)e^{j2\pi kf_st} + v_2(t)e^{-j2\pi kf_st}, \tag{2.7}$$

where v_0 is the input signal from radiator element, v_1 and v_2 are the inputs from parasitic elements, kf_s is the oscillator circuit frequency controlled by the variable reactance.

To achieve an optimum antenna radiation elevation pattern, the ESPAR antenna structure must be designed as shown in the Fig. 2.8 [13]. For a transmission

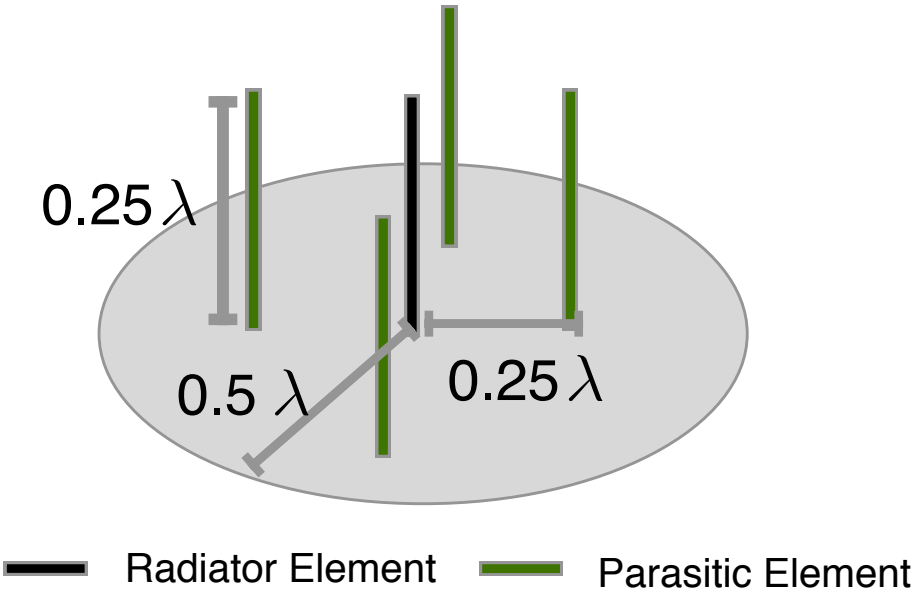

Figure 2.8: ESPAR antenna configuration for optimum elevation pattern

RF signal with λ wavelength, the configuration of the ESPAR antenna is as below:

- The circular ground planar radius is equal to 0.5 λ.
- Antenna element length is 0.25 λ.
- Spacing between radiator element and parasitic element is 0.25 λ.
- Radius of antenna element is 0.01 λ.

3 Channel Estimation for OFDM Systems with ESPAR Antenna

This chapter presents the channel estimation for the OFDM system with ESPAR antenna. The chapter 3.1 shows the system model and mathematical representation of the channel estimation problem in the ESPAR-OFDM system. The chapter 3.2 presents the current compressed sensing based channel estimation for the ESPAR-OFDM system. The chapter 3.3 explains the computational complexity problem in the current compressed sensing based channel estimation for ESPAR-OFDM ssytem.

3.1 System Model

In the conventional OFDM system, the receiver can exploit the structure of the diagonal channel matrix to estimate the CSI. The channel estimation acquires pilot tones which are inserted into the transmitted signal. Pilot tones are BPSK signals which known in both the transmitter and receiver. Basically there are two types of the pilot insertion, block type and comb type insertion as shown in the Fig. 3.1.

The block type pilot insertion is also considered as a preamble. In this type of the insertion, all the pilot tones occupy all the sub-carrier in one transmission time slot. Using this method, the CSI can be fully recovered by a simple division operation at the receiver side. This method is suitable for a slow fading channel when the CSI not rapidly changing over time. The block type pilot also can be used to do the synchronization at the receiver side to detect the delay difference of the clock of the receiver and the transmitter.

The comb type pilot insertion is done by inserting the pilot in the several sub-

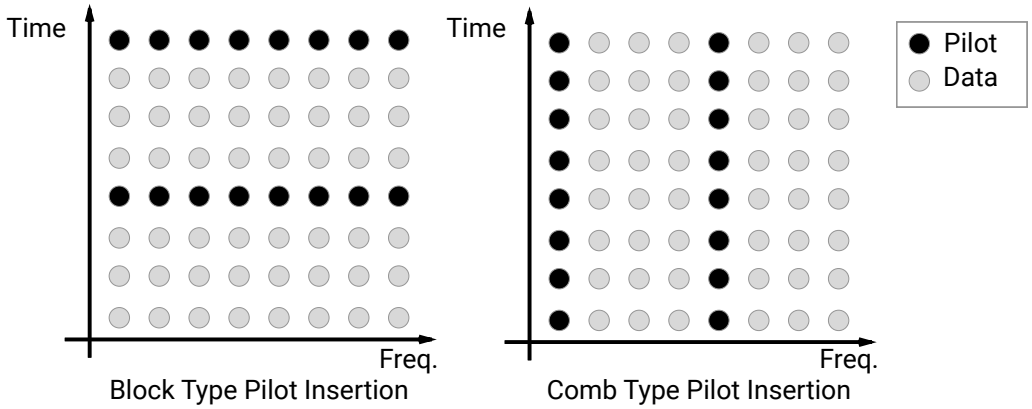

Figure 3.1: Pilot arrangement types

carrier tones in every transmission time slot. This method is suitable for the fast fading channel where the channel changing in almost of every OFDM symbol. The pilot tones are distributed evenly in the OFDM sub-carriers, thus in order to obtain the complete CSI an interpolation method is necessary.

To get the frequency domain CSI, the receiver needs to separate the pilot tones from the demodulated signal. Then, by using the known transmitted pilot value, an observation vector $\mathbf{H}_{ob}$ can be calculated as

$$\mathbf{H}_{ob} = \frac{\mathbf{Y}_{((i-1)(S/T))}}{\mathbf{X}_{((i-1)(S/T))}}, \qquad i = 1,2,3...,T \tag{3.1}$$

where T is number of the pilot tones. The observation points are spreading evenly in the frequency domain CSI [53]. Because of that, to get the unknown CSI values, receiver can utilize an interpolation method between two observation points [54]. After the equalization, then the receiver can utilize multilevel QAM de-mapper to convert the signal into its original bit stream form. The CSI after the channel estimator then are used recovers the $\mathbf{H}_{eq}$ matrix, the equalization process can be performed to remove the fading effect. Finally, the M-QAM demapper will demodulate the sub-carrier symbols into the bit stream.

The block diagram structure of the OFDM system using ESPAR antenna is shown in Fig. 3.2. In this dissertation, we use 3-element ESPAR antenna, with one radiator element and two parasitic elements. The varactor at each pair of the parasitic elements are adjusted so that its oscillator circuit has an alternate directivity as sine and cosine with the same f_s frequency. The element with the

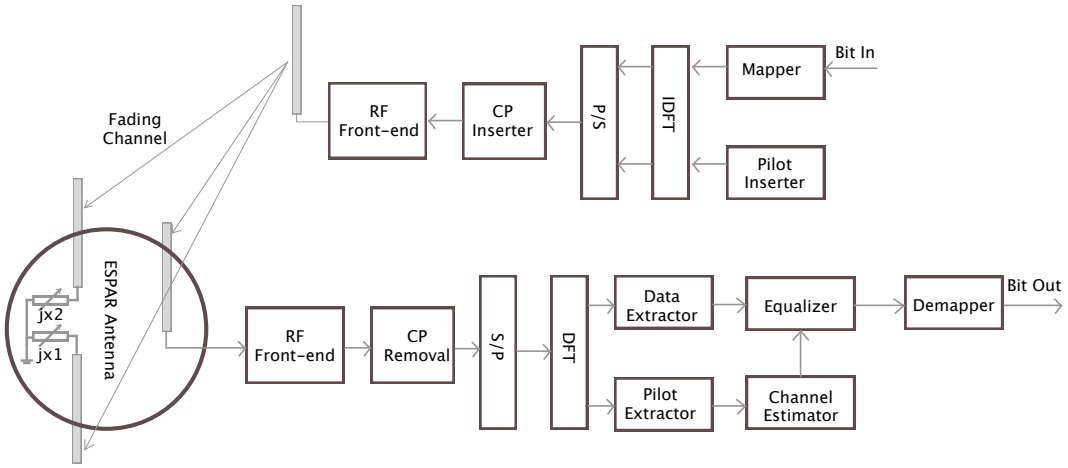

Figure 3.2: System model of the OFDM system with ESPAR antenna.

cosine oscillator is called the positive shifted element and the negative shifted element for the element with sine oscillator.

The transmitter part is the same with the conventional OFDM. The input bit stream is mapped by the multilevel quadrature amplitude modulation (M-QAM). Then pilot sub-carriers are inserted in this data sub-carrier. The transmitter uses IDFT to generate the OFDM symbol. Before the OFDM symbol is transmitted trough the multipath channel, the cyclic prefix (CP) is inserted to the OFDM symbol by copying a certain part of the symbol's rear to its front. CP has a purpose to prevent the inter-symbol interference (ISI). Moreover, CP removal at the receiver side will create a cyclic form of the channel matrix, similar to the SISO-OFDM as shown in the Eq. 2.2. Thus, the frequency domain $\mathbf{H}$ matrix will be a diagonal as shown in Eq. 2.4.

The received signal at each antenna element will have an independent CIR. Moreover, the signals at each parasitic elements will be oscillated to create the diversity. A pair of $cos(2\pi f_s t)$ and $sin(2\pi f_s t)$ applied to the received signal at each parasitic element. The final received sub-carrier ($\mathbf{Y}$), that goes to the demodulator part, can be defined as

$$\mathbf{Y} = \mathbf{F}(\mathbf{g}_p\mathbf{h}_p + \mathbf{h}_0 + \mathbf{g}_n\mathbf{h}_n)\mathbf{F}^H\mathbf{X}, \tag{3.2}$$

where vector $\mathbf{X} \in \mathbb{C}^N$ is the transmitted sub-carrier, $\mathbf{h}_0 \in \mathbb{C}^{N\times N}$,$\mathbf{h}_p \in \mathbb{C}^{N\times N}$, and $\mathbf{h}_n \in \mathbb{C}^{N\times N}$ are the time domain CIR for radiator, positive shifted and negative

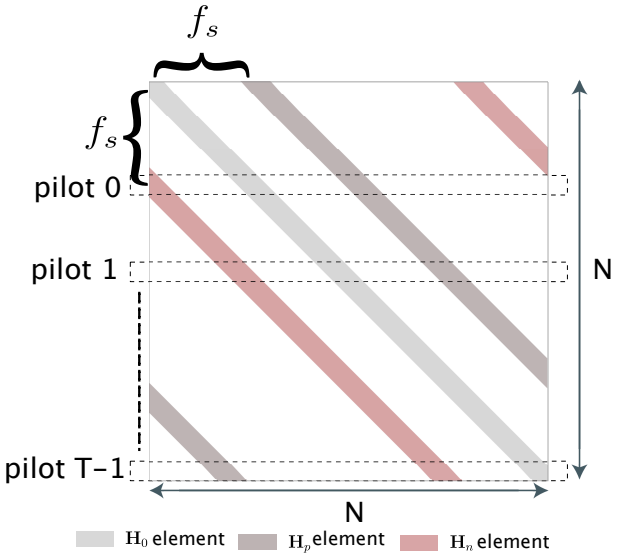

Figure 3.3: Equivalent frequency domain channel matrix $\mathbf{H}_{eq}$.

shifted element respectively. Matrices $\mathbf{g}_p \in \mathbb{C}^{N\times N}$ and $\mathbf{g}_n \in \mathbb{C}^{N\times N}$ are diagonal matrices form of $cos(2\pi f_s t)$ and $sin(2\pi f_s t)$ respectively. Using Eq. (2.3), the frequency domain form of Eq. (3.2) can be redefined as

$$\mathbf{Y} = (\mathbf{G}_p\mathbf{H}_p + \mathbf{H}_0 + \mathbf{G}_n\mathbf{H}_n)\mathbf{X}, \tag{3.3}$$

where matrices $\mathbf{H}_0 \in \mathbb{C}^{N\times N}$, $\mathbf{H}_p \in \mathbb{C}^{N\times N}$ and $\mathbf{H}_n \in \mathbb{C}^{N\times N}$ are the frequency domain channel matrices for radiator, positive shifted, and negative shifted element respectively. The $\mathbf{G}_p \in \mathbb{C}^{N\times N}$ and $\mathbf{G}_n \in \mathbb{C}^{N\times N}$ are shift matrices with alternate directivity of frequency f_s.

The equivalent channel matrix ($\mathbf{H}_{eq} \in \mathbb{C}^{N\times N}$) in this transmission can be defined as

$$\mathbf{H}_{eq} = (\mathbf{G}_p\mathbf{H}_p + \mathbf{H}_0 + \mathbf{G}_n\mathbf{H}_n). \tag{3.4}$$

Fig. 3.3 shows a more detail structure of the equivalent channel matrix. Because the matrix is no longer diagonal, a channel estimation with the interpolation method cannot be applied here. Moreover, to prevent the inter-carrier interference between pilot and data sub-carrier, the oscillator frequency (f_s) at each parasitic element is adjusted to be equal to the pilot spacing. For ESPAR-OFDM system

the channel estimator need to estimate the CIR for each antenna element. For 3-elements ESPAR antenna, the CIR can be defined as

$$\mathbf{e} = [\mathbf{e}_p \, \mathbf{e}_0 \, \mathbf{e}_n]^T. \tag{3.5}$$

here the $\mathbf{e}_0 \in \mathbb{C}^L$, $\mathbf{e}_p \in \mathbb{C}^L$, and $\mathbf{e}_n \in \mathbb{C}^L$ are the CIR from radiator, positive and negative parasitic element respectively.

3.2 Compressed Sensing based Channel Estimation

3.2.1 Compressed Sensing

Recently, compressed sensing (CS) has became a new prominent technique in channel estimation [55–58]. Compressed sensing is a new data acquisition technique that enables the reconstruction of a sparse signal with sub-Nyquist samples [25], [26]. The implementation of CS based channel estimation in the OFDM system is offering better accuracy and less pilot utilization. The core of CS algorithms is to find the locations of the non-zero elements in sparse signal. There are two main groups of compressed sensing approach, basis pursuit and greedy pursuit [59]. Basis pursuit algorithms acquire L_p-norm to find all the locations of the non-zero element at once. While, greedy pursuit algorithms use the iterative method to get the locations. In most cases, the greedy pursuit will have some performance degradation compared to that of basis pursuit. However, it offers a lower cost of computation. The major greedy algorithms are matching pursuit (MP) and orthogonal matching pursuit (OMP). MP has the least complexity among all the CS algorithms, but it requires a high number of iterations in its process [60]. OMP reduces MP's high iterations number by acquiring least-squares in every step of its iteration, thus, it can avoid choosing the same location of non-zero element twice [61]. OMP is preferable in real-time application because it provides a short execution time. However, the implementation of OMP algorithm still requires a heavy cost of computation for its sensing matrix multiplication and least-squares computation.

The main purpose of the CS algorithm is to allow a signal reconstruction with the sub-Nyquist samples. Hence, its sampling process can be described as an under-determined linear system as

$$\mathbf{b} = \mathbf{\Psi a} + \mathbf{w}, \tag{3.6}$$

where $\mathbf{\Psi} \in \mathbb{C}^{N \times M}$ is the sensing matrix, $\mathbf{a} \in \mathbb{C}^{M \times 1}$ is the reconstructed signal, $\mathbf{b} \in \mathbb{C}^{N \times 1}$ is the sampled signal, N is the number of samples and $N < M$. However, if signal $\mathbf{a}$ is sparse, we can neglect the columns in matrix $\mathbf{\Psi}$ that correspond to the zero elements. Consequently, the overall system in Eq. (3.6) can be a determined linear system.

As proposed by Donoho in [25], the CS algorithm can utilize the inner product of a matrix that has a restricted isometric property (RIP) to locate the non-zero element location α in the sparse signal $\mathbf{a}$ as

$$\alpha = \underset{i=1...M}{\arg\max} |\langle \mathbf{\Psi}_i^H, \mathbf{b} \rangle|, \tag{3.7}$$

where $\mathbf{\Psi}_i^H$ is the i-th row in the matrix $\mathbf{\Psi}^H$. The RIP matrix multiplication holds a special property where the location of its maximum result α will also be the location of one of the non-zero elements in signal $\mathbf{a}$.el

The wireless communication system is a real-time application that requires strict execution time for its processes, greedy pursuit based CS algorithm is a good practical approach to met fast reconstruction time with acceptable hardware complexity. This research choose orthogonal matching pursuit (OMP) which is one of the prominent greedy pursuit based CS algorithms that offer small iteration number and good reconstruction performance [61].

Algorithm 1 shows the detail of the OMP computation. After the initialization step, every iteration will require inner product computation. The sensing matrix inner product as in Eq. (3.7) is the requirement for every CS algorithm to get the locations of the non-zero elements. The $\mathbf{\Phi}$ matrix will hold the columns from $\mathbf{\Psi}$ that correspond to the sparse locations. Next, OMP uses least-squares to get the approximate solution for the current set of non-zero element locations. To evaluate this current solution, a residue is computed as in the step 11 of Algorithm 1. The residue is the subtraction of the sampled signal $\mathbf{b}$ with the current solution contribution ($\mathbf{\Phi}_t \mathbf{a}$). If the residue value satisfies the stopping criterion, the current

Algorithm 1 OMP Algorithm

1: *init*:
2: $\mathbf{r} \leftarrow \mathbf{b}; \mathbf{\Phi}_0 \leftarrow [\quad]$
3: *loop*:
4: $\quad \mathbf{g} \leftarrow \langle \mathbf{\Psi}^H, \mathbf{r} \rangle$
5: $\quad \alpha \leftarrow \arg\max_{i=1...M} |\mathbf{g_i}|$
6: $\quad$ *augment*:
7: $\quad \mathbf{\Phi}_t \leftarrow \mathbf{\Phi}_{t-1} | \mathbf{\Psi}_\alpha^H$
8: $\quad$ *least square*:
9: $\quad \mathbf{a} \leftarrow arg\ min_a ||\mathbf{r} - \mathbf{\Phi}_t \mathbf{a}||^2$
10: $\quad$ *update*:
11: $\quad \mathbf{r} \leftarrow \mathbf{b} - \mathbf{\Phi}_t \mathbf{a}$
12: **if** the stopping criterion of $\mathbf{r}$ is not met **goto** *loop*.

approximate solution can become the final output. In contrast, If the stopping criterion cannot be met, OMP will require an additional iteration. This residue will be the input for the next inner product multiplication. Since the current solution contribution has been removed from the residue, the maximum inner product result will always be calculated for the new location.

However, compared to the interpolation method, the implementation of OMP will still raise the hardware's resources. There are two main operations in OMP that require a high computational complexity, the inner product multiplication in step 4 and the least-squares in step 9 of Algorithm 1. Since the $\mathbf{\Psi}^H$ matrix has $M \times N$ dimension, its multiplication will also require at least $M \times N$ number of complex multipliers. In the OFDM system case, this multipliers requirement will become very high that make it hard to be realized in a mobile system. The practical approach is to compute the matrix multiplication iteratively row by row as proposed in [27] and [30]. However, the iterative method has a drawback of long hardware cycle period.

The most common way to solve the least-squares problem is using the matrix inversion. Furthermore, the combination of the QR decomposition and the backward substitution can provide a less complex solution for the matrix inversion. In this paper we use givens rotations for the QR decomposition method

Algorithm 2 Givens Rotations Algorithm

1: *input*: $\mathbf{A} \in \mathbb{C}^{d \times d}$
2: The givens algorithm create $\mathbf{Q}^H \mathbf{A} = \mathbf{R}$
3: *loop*:
4: *for* i=1; i≤d; i++;
5: *for* j=d; j≥i; j--;
6: $Ve^{j\theta_a} = \mathbf{A}(j-1, i)$
7: $Ze^{j\theta_b} = \mathbf{A}(j, i)$
8: $\theta_1 = tan^{-1}(V/Z)$
9: $\mathbf{A}_{tmp} = \mathbf{A}(j-1 : j, i : d)$
10: $\mathbf{A}_{tmp} = \begin{bmatrix} cos\theta_1 e^{-j\theta_a} & sin\theta_1^{-j\theta_b} \\ -sin\theta_1^{-j\theta_a} & cos\theta_1^{-j\theta_b} \end{bmatrix} \mathbf{A}_{tmp}$
11: $\mathbf{A}(j-1 : j, i : d) = \mathbf{A}_{tmp}$
12: *end for*
13: *end for*

which is shown in Algorithm 2. This algorithm decomposes $\mathbf{A}$ matrix into upper triangular matrix $\mathbf{R}$ using a series of rotation matrix multiplications. Every iteration of this algorithm will change the element $\mathbf{A}(j, i)$ to be zero. The step 5 to step 8 are to define the phase difference between the element $\mathbf{A}(j, i)$ and its lower row element $\mathbf{A}(j-1, i)$. An rotation matrix which this phase difference is multiplied to the whole elements in row j and $(j-1)$. In this algoritm we use a temporary matrix $\mathbf{A}_{tmp}$ to address all the non zero elements in these j-th and $(j-1)$-th rows. The whole processes are repeated for every pair of elements in lower diagonal parts until matrix $\mathbf{A}$ becomes triangular. Then, the inversion of this triangular matrix can utilizes backward substitution easily. This algorithm has an advantage in hardware implementation because the series of rotation matrix multiplications can be realized with a systolic array of coordinate rotation digital computer (CORDIC) [62].

The implementation of CS algorithm in OFDM channel estimation can lead to better channel reconstruction quality and less pilot utilization. To apply the CS algorithm in OFDM channel estimation, we need to redefine the observation vector in Eq. (3.1) as an multiplication of a RIP matrix with a sparse signal as in

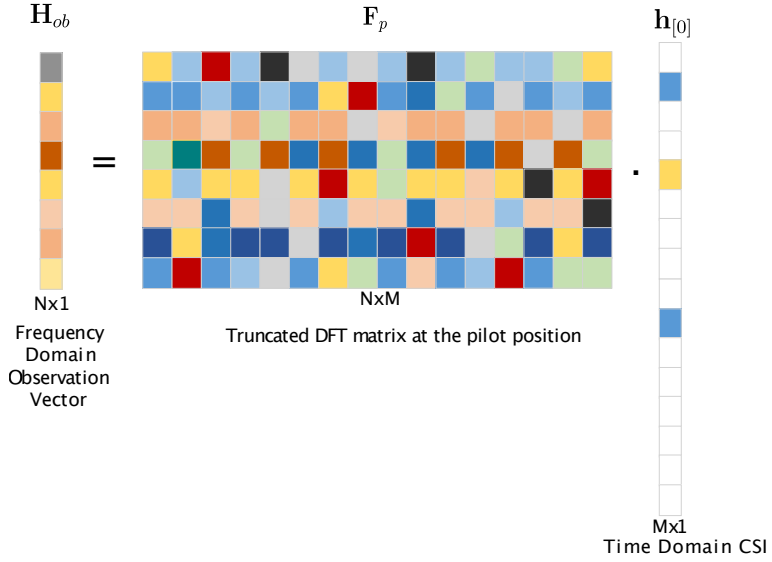

Figure 3.4: Compressed sensing representation for OFDM channel estimation problem

Eq. (3.6). Because CSI is sparse in the time domain [63], the sparse requirement can be met by changing the frequency domain CSI into time domain one as

$$\mathbf{H} = diag(\mathbf{F}\mathbf{h}_{[0]}), \tag{3.8}$$

where $\mathbf{h}_{[0]}$ is the time domain CIR as described in the chapter 2.2. The Eq. (3.1) then can be redefined as

$$\mathbf{H}_{ob} = \mathbf{F}_P\mathbf{h}_{[0]} + \mathbf{W}. \tag{3.9}$$

where $\mathbf{F}_P \in \mathbb{C}^{N\times M}$ is a truncated DFT matrix. The row elements of $\mathbf{F}_P$ are from the DFT matrix rows that correspond to the pilot positions, and N equals to T as number of pilots. Because the receiver is only able to equalize a signal with maximum delay spread less than CP, the column elements of $\mathbf{F}_P$ can be chosen to be the first M columns of DFT matrix that correspond to the CP length. Now, Eq. (3.9) has met all the CS requirements, as $\mathbf{H}_{ob}$ is the sampled vector, $\mathbf{h}_{[0]}$ is the sparse reconstructed signal and $\mathbf{F}_P$ is the sensing matrix [64]. The CS representation of this OFDM channel estimation is shown in Fig. 3.4.

The CP and pilot configuration will influence the structure of the sensing matrix $\mathbf{F}_P$. CP length will define the number of column in the $\mathbf{F}_P$ matrix and the number

of pilot will determine the row length in the $\mathbf{F}_P$ matrix. The size of $\mathbf{F}_P$ matrix is closely related to the complexity in both inner product and least square operation in the OMP algorithm. Moreover, in term of reconstruction performance, the structure of the sensing matrix will define the number of path that the system can reconstruct [65].

3.2.2 Compressed Sensing in ESPAR-OFDM System

CS with OMP has been proposed as a solution to the channel estimation problem in the ESPAR-OFDM system [22]. The channel estimation can be modeled as a compressed sensing underdetermined linear system problem, where the sensing matrix is the union of multiple Fourier matrices proportional to the number of the antenna element. The OMP computation can be divided into two main parts. First, the inner product computation to obtain the sparse CIR locations. The maximum value from the sensing matrix and the observation vector multiplication will hold the location of the CIR. Second main part is the CIR reconstruction with the least square method. Using the known CIR locations, the least square is simplified as only the columns of sensing matrix that correspond to the sparse element involved. Since the CIR is sparse, the matrix size will be greatly reduced for the least square.

Let us define the channel estimation problem from the following equation as

$$\mathbf{B} = \mathbf{\Psi a} + n, \tag{3.10}$$

where $\mathbf{B}$ is the sampled signal, $\mathbf{a}$ is the sparse reconstructed signal, n is the AWGN noise and $\mathbf{\Psi}$ is the sensing matrix. The sampled signal $\mathbf{B}$ which is used for channel estimation can be defined as an observation vector as

$$\mathbf{B} = (\mathbf{G}_p^c\mathbf{H}_p^c + \mathbf{H}_0^c + \mathbf{G}_n^c\mathbf{H}_n^c)\mathbf{P}, \tag{3.11}$$

where $(.)^c$ is the truncated matrix which only includes the matrix elements that related to the pilot locations in both row and column direction. The size of each truncated matrix $(.)^c$ is supposed as $T \times T$, where T is the pilot or observation vector number. Here, the vector $\mathbf{P} \in \mathbb{R}^{T\times 1}$ is the pilot vector. Using the unfolding technique, we can rewrite Eq. (3.11) as

$$\mathbf{B} = \left[\mathbf{G}_p^c\mathbf{H}_p^c\ \mathbf{H}_0^c\ \mathbf{G}_n^c\mathbf{H}_n^c\right]\left[\mathbf{P}\ \mathbf{P}\ \mathbf{P}\right]^T. \tag{3.12}$$

Algorithm 3 Multi-column OMP Algorithm

input: $\mathbf{B}; \mathbf{\Psi}$
init: $\mathbf{r} \leftarrow \mathbf{B}; t \leftarrow 0; \mathbf{\Phi}_0 \leftarrow [\,];$
loop:
    $\alpha \leftarrow arg\ max|\langle \mathbf{\Psi}^H, \mathbf{r} \rangle|$
    $l \leftarrow \alpha \mod L$
    create index set $\Omega \leftarrow \alpha + i * L; i = 0, 1, 2, ..A_t$
    augment:
    $\mathbf{\Phi}_t \leftarrow \mathbf{\Phi}_{t-1} | \mathbf{\Psi}^H_{\mathbf{\Omega}}$
    least square:
    $\mathbf{a} \leftarrow arg\ min||\mathbf{b} - \mathbf{\Phi}_t \mathbf{a}||^2$
update:
$\mathbf{r} \leftarrow \mathbf{b} - \mathbf{\Phi}_t \mathbf{a}$
$t \leftarrow t + 1$
if stoping criterion not met **goto loop**.

Because of the diagonal structure of channel matrices $\mathbf{H}_p$, $\mathbf{H}_0$ and $\mathbf{H}_n$, the channel estimation equation can be derived as

$$\mathbf{B} = \begin{bmatrix} \mathbf{G}^c_p \mathbf{P} & \mathbf{P} & \mathbf{G}^c_n \mathbf{P} \end{bmatrix} \begin{bmatrix} diag(\mathbf{H}^c_p) \\ diag(\mathbf{H}^c_0) \\ diag(\mathbf{H}^c_n) \end{bmatrix}. \tag{3.13}$$

The diagonal of channel matrix $\mathbf{H}$ can be derived from the CIR as

$$diag(\mathbf{H}) = \mathbf{F}\mathbf{e}, \tag{3.14}$$

where $\mathbf{e}$ is the CIR from the first column of the matrix $\mathbf{h}$. Using Eq. (3.14), the Eq. (3.13) can be modified as

$$\mathbf{B} = \begin{bmatrix} \mathbf{G}^c_p \mathbf{P} \mathbf{F}_L & \mathbf{P} \mathbf{F}_L & \mathbf{G}^c_n \mathbf{P} \mathbf{F}_L \end{bmatrix} \begin{bmatrix} \mathbf{e}_p \\ \mathbf{e}_0 \\ \mathbf{e}_n \end{bmatrix}, \tag{3.15}$$

where $\mathbf{F}_L \in \mathbb{R}^{T \times L}$ is a partial DFT matrix which its T row vectors are from DFT matrix according to the pilot locations and each row vector just includes the first L values of DFT vectors related to the CP length.

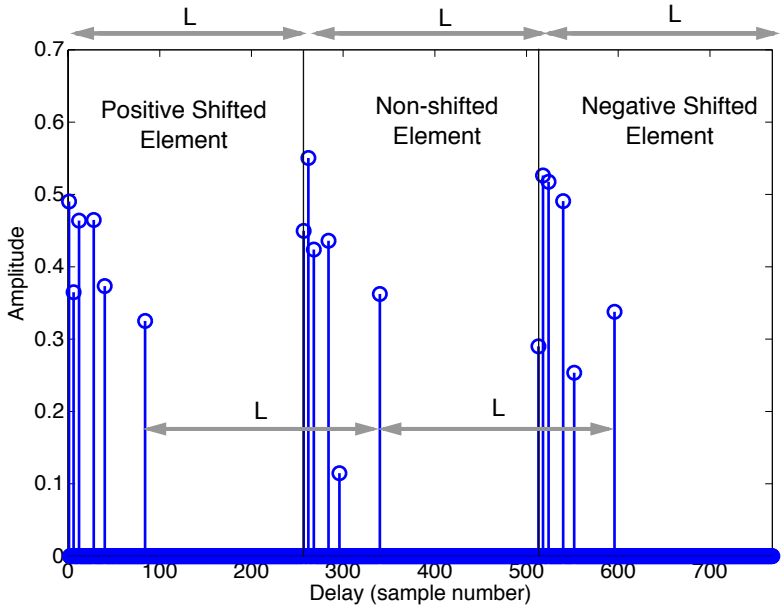

Figure 3.5: Expected CIR ($\mathbf{a}$) reconstruction result

Finally we can define the sensing matrix $\mathbf{\Psi} \in \mathbb{C}^{T \times 3L}$ as

$$\mathbf{\Psi} = \left[\mathbf{G}_p^c \mathbf{P}\mathbf{F}_L \ \mathbf{P}\mathbf{F}_L \ \mathbf{G}_n^c \mathbf{P}\mathbf{F}_L\right], \tag{3.16}$$

Then, the sparse reconstructed signal $\mathbf{a} \in \mathbb{C}^{3L \times 1}$ is defined as

$$\mathbf{a} = \left[\mathbf{e}_p \ \mathbf{e}_0 \ \mathbf{e}_n\right]^T. \tag{3.17}$$

Fig. 3.5 shows the structure of the expected CIR ($\mathbf{a}$) reconstruction result from the channel estimation. The vector $\mathbf{a}$ consists of three component, positive shifted, non-shifted and negative shifted element. Each component has a length of L.

Because each antenna element is close to each other (less than 1 λ) as shown in Fig. 2.8, we can assume the sparse locations on each CIR are the same. The reference [23] proposed a multi-column OMP by exploiting this property as shown in Alg. 3. The main difference of multi-column OMP with the conventional OMP lies in the Step 4 and 5. As shown in the Fig. 3.5, if the each component has the same delay profile, then we only need to get the relative delay profile and retrieve the delay profile for all the CIR components by adding 0 for positive shifted part,

L for non-shifted part and $2L$ for negative shifted part. In the Step 4, when a location of a non-zero element is found in a sub-set CIR, the CS need to get the relative location by applying a modulo operation with L. Then, in the Step 5, the proposed multi-column OMP can calculate multiple non-zero elements location at once from Step 4. Therefore, the total number of iteration involved in the OMP computation can be largely reduced. However, the sensing matrix involves in the multi-column OMP computation still has a huge size and requires huge computational complexity. Reader can find the detail of multi-column OMP for ESPAR antenna system in [22].

3.3 Computational Complexity

The computational cost to compute the multi-column OMP algorithm from the Algorithm. 3 in OFDM system with A_n elements ESPAR antenna is shown in the Table. 3.1. The main bottleneck in the multi-column OMP is the inner product computation where it need to compute a multiplication with a huge matrix with the size of A_nTL. Where, the latter part after the inner product, the OMP only need to deal with a much smaller truncated matrix which defined by the CIR locations.

The usual approach to perform the inner product is by performing the matrix multiplication row by row as proposed in [27–30]. Thus, to perform one inner product it will require A_tL number of iterations. This will lead to a very long computational time in each iteration of Algorithm. 3. In results, it will be very hard to meet the real-time timing requirement, which required the channel estimation to be done between CP period.

Table 3.1: Computational cost for the multi-column OMP per Iteration.

No	Term	$\times$	/	CORDIC
1.	$\mathbf{g} = \langle \mathbf{\Psi}_N^H, \mathbf{r} \rangle$	$A_n T L$		
2.	$\alpha = arg\ max \lvert \mathbf{g} \rvert$	$A_n L$		
3.	$\mathbf{\Omega} = [\alpha + iL]$	-	-	-
4.	$\mathbf{\Phi}_t = \mathbf{\Phi}_{t-1} \lvert \mathbf{\Psi}_{\mathbf{\Omega}}^H$	-	-	-
5.	$\mathbf{b}_t = \mathbf{\Phi}^H b$	$A_n T$		
6.	$\mathbf{S} = \mathbf{\Phi}^H \mathbf{\Phi}$	-	-	-
7.	$\mathbf{S}^{-1} = inv(\mathbf{S})$	-	-	$\frac{(A_n^2 \kappa^2 + A_n \kappa)}{2}$
8.	$\mathbf{a} = \mathbf{S}^{-1} \mathbf{b}_t$	$(A_n^2 \kappa^2 - A_n \kappa)/2$	$A_n \kappa$	-
9.	$\mathbf{r} = \mathbf{b} - \mathbf{\Phi}_t \mathbf{a}$	$A_n T$		
	Total	$A_n T L + A_n L + 2A_n T + (A_n^2 \kappa^2 - A_n \kappa)/2$	$A_n \kappa$	$\frac{(A_n^2 \kappa^2 + A_n \kappa)}{2}$

4 Computational Complexity Reduction Methods

This chapter provides the OMP algorithm modification in the ESPAR-OFDM system to achieve lower complexity. The OMP computation for the channel estimation in the ESPAR-OFDM system has a huge sensing matrix which size is also determined by the number of the antenna element. However, the full size of the sensing matrix only used in the inner product computation in order to detect CIR delay location as shown in the Alg. 3. While, in the latter processes, the OMP only need to deal with the truncated matrix ($\mathbf{\Phi}$). Matrix $\mathbf{\Phi}$ size is equal to the $T \times 3\kappa$, where κ is the number of sparsity in the CIR. Compare to the matrix $\mathbf{\Psi}$ which size $T \times 3L$, the size of matrix $\mathbf{\Phi}$ is extremely small. Because of that, we can say that the bottleneck of the multi-column OMP in the Alg 3 is lies at the inner product computation in the step 4.

There are several unique properties that we can exploit to reduce the inner product computational complexity. First, because the CIR delay profile is the same for all antenna element, we propose a modified multi-column OMP method. Here, we introduce a new sensing matrix which size is $T \times L$, smaller compared to the original $T \times 3L$ size matrix $\mathbf{\Psi}$. We present the detail of the modified multi-column OMP in the sub-section 4.1. Second, because of the sensing matrix is based on the DFT matrix, we can exploit its symmetrical property to apply the matrix strength reduction. Using this method we can further reduce the sensing matrix size to be $Q \times R$. The detail of Q will be presented in the sub-section 4.2. Third, due to the nature of the CS algorithm itself which can work with small number of measurement, we propose a observation vector selection method to reduce the row size of the sensing matrix. The combination of the 3 methods can suppress the size of the sensing matrix into $R \times Q$, the detail of the parameter R

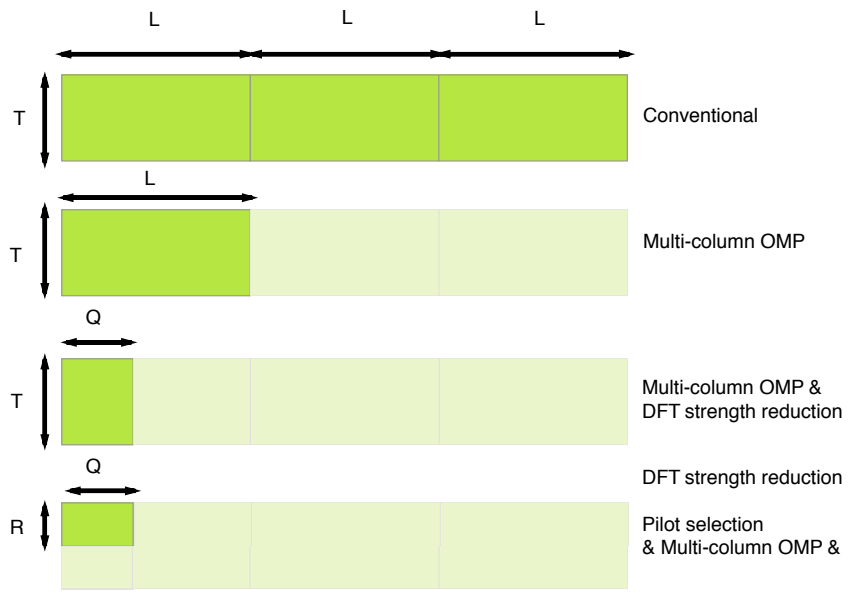

Figure 4.1: General description of the propose methods for sensing matrix reduction

is presented in the sub-section 4.3. General description of the 3 propose methods can be seen in Fig. 4.1.

4.1 Multi-column OMP

The CIR delay profile of each antenna element are the same. Accordingly, the maximum value from the inner product projection of each 3 sub-matrices will have the same relative location. Instead of only exploit this property to reduce the number of iteration as proposed in [22,23], we propose a modification in result to a reduction in both iteration time and multiplier number. To achieve that, in this paper we introduce a new sensing matrix which is an overlap of the 3 sub-matrices as

$$\mathbf{\Psi}_N = \mathbf{G}_p^c \mathbf{P}\mathbf{F}_L + \mathbf{P}\mathbf{F}_L + \mathbf{G}_n^c \mathbf{P}\mathbf{F}_L. \tag{4.1}$$

The new sensing matrix will have a dimension of $T \times L$, which is equal to only one sub-element of the original sensing matrix $\mathbf{\Psi}$. The multiplication results value itself is not necessarily required in the OMP inner product, as we only interested

in the maximum value location. The new sensing matrix $\mathbf{\Psi_N}$ will combine the inner product result from each sub-matrices. It will change the multiplication result, but the maximum value location will remain the same.

Algorithm 4 Modified multi-column OMP algorithm

1: *input*: $\mathbf{b}; \mathbf{\Psi}; \mathbf{\Psi}_N$
2: *init*: $\mathbf{r} \leftarrow \mathbf{b}; t \leftarrow 0; \mathbf{\Phi}_0 \leftarrow [\,]$;
3: **loop**:
4: $\quad \alpha \leftarrow arg\ max|\langle \mathbf{\Psi}_N^H, \mathbf{r} \rangle|$
5: $\quad$ create index set $\mathbf{\Pi} \leftarrow \alpha + \alpha * L; i = 0, 1, 2, .., A_t$
6: $\quad$ *augment*:
7: $\quad \mathbf{\Phi}_t \leftarrow \mathbf{\Phi}_{t-1}|\mathbf{\Psi}_{\mathbf{\Pi}}^H$
8: $\quad$ *least square*:
9: $\quad \mathbf{a} \leftarrow arg\ min||\mathbf{b} - \mathbf{\Phi}_t\mathbf{a}||^2$
10: *update*:
11: $\mathbf{r} \leftarrow \mathbf{b} - \mathbf{\Phi}_t\mathbf{a}$
12: $t \leftarrow t + 1$
13: **if** stoping criterion not met **goto loop**.

Using the new sensing matrix, we can specify the modified multi-column OMP as shown in the Alg. 4. In this propose method, beside the original sensing matrix $\mathbf{\Psi}$, there will be an additional new matrix $\mathbf{\Psi}_N$ at the input part. Then, the inner product at the step 4 will use the matrix $\mathbf{\Psi}_N$ instead of matrix $\mathbf{\Psi}$. The modulo operation at the step 5 of the Alg. 3 is unnecessary as the maximum value location already represent the relative distance for each sub-matrices element. In each iteration, the modiified multi-column OMP add A_t indices to the vector $\mathbf{\Pi}$. For 3 elements ESPAR, the set of indices can be obtained by adding 0, L and $2L$ to the maximum projection result α from the step 4. The 3 indices is used to truncate 3 columns of the original sensing matrix $\mathbf{\Psi}$ into matrix $\mathbf{\Phi}$. Accordingly, the expected CIR vector $\mathbf{a}$ will grow 3 times faster at each iteration.

The modified 3C-OMP will keep the advantage of the original 3C-OMP as multiple of CIR locations can be detected at each iteration. Furthermore, the number of multipliers in the inner product computation can be reduced from $3TL$ into TL. The implementation of this method in the OFDM system with 3-element

ESPAR antenna can reduce both of the iteration and the multiplier number. For the 3-element ESPAR antenna, this method can bring 66% reduction to the inner product computation. However, the possibility to implement this method into the ESPAR antenna with larger elements can result to a greater impact of reduction.

Using the distributive property of the matrix multiplication, we can further decompose the new sensing matrix from the Eq. 4.1 into

$$\mathbf{\Psi}_N = (\mathbf{G}_p^c\mathbf{P} + \mathbf{P} + \mathbf{G}_n^c\mathbf{P})\mathbf{F}_L. \tag{4.2}$$

Then, the inner product computation can be redefined as

$$|\langle \mathbf{\Psi}_N^H, \mathbf{r}\rangle| = |\langle \mathbf{F}_L^H(\mathbf{G}_p^c\mathbf{P} + \mathbf{P} + \mathbf{G}_n^c\mathbf{P})^H, \mathbf{r}\rangle|. \tag{4.3}$$

Now, let define vector $\mathbf{\Theta}$ as

$$\mathbf{\Theta} = (\mathbf{G}_p^c\mathbf{P} + \mathbf{P} + \mathbf{G}_n^c\mathbf{P})^H\mathbf{r}. \tag{4.4}$$

Vector $\mathbf{\Theta}$ is easy to compute as it only a combination of three shifted vector $\mathbf{r}$ which consist of ones and zeros. Now we can redefine the inner product computation again as

$$|\langle \mathbf{\Psi}_N^H, \mathbf{r}\rangle| = |\langle \mathbf{F}_L^H, \mathbf{\Theta}\rangle|. \tag{4.5}$$

Here, an additional memory usage to store the new sensing matrix $\mathbf{\Psi_N}$ is not necessary as the matrix $\mathbf{F}_L^H$ can be retrieved from the non-shifted element of the matrix $\mathbf{\Psi}$.

4.2 DFT Matrix Strength Reduction

The main complexity for the inner product from the Eq. 4.5 is the matrix $\mathbf{F}_L^H$, since the $\mathbf{P}$ matrix only consist of BPSK signal of 1 and -1. The matrix $\mathbf{F}_L^H$ is a truncated DFT matrix in both column and row direction, because of that the FFT algorithm may not give an efficient hardware implementation result. However, some of the symmetrical property of the DFT will remain in this matrix. Moreover, the size of the matrix $\mathbf{F}_L^H$ is smaller than a full DFT matrix. The matrix strength reduction technique as proposed in ref. [34] can be implemented in the

matrix $\mathbf{F}_L^H$ multiplication to achieve even lower complexity compare to the full FFT technique.

The measurement matrix has some unique properties which inherited from DFT matrix. Let us describe the measurement matrix $\mathbf{\Omega}$ as the Hermitian of $\mathbf{\Psi}$ matrix represented as

$$\begin{aligned}\mathbf{\Omega} &= \mathbf{F}_L^H \\ &= \begin{bmatrix} \omega^0 & \omega^0 & \omega^0 & \cdots & \omega^0 \\ \omega^0 & \omega^p & \omega^{2p} & \cdots & \omega^{(T-1)p} \\ \omega^0 & \omega^{2p} & \omega^{4p} & \cdots & \omega^{2(T-1)p} \\ \omega^0 & \omega^{3p} & \omega^{6p} & \cdots & \omega^{3(T-1)p} \\ \omega^0 & \omega^{4p} & \omega^{8p} & \cdots & \omega^{4(T-1)p} \\ \vdots & \vdots & \vdots & \vdots & \vdots \\ \omega^0 & \omega^{Lp} & \omega^{2Lp} & \cdots & \omega^{(L-1)(T-1)p} \end{bmatrix},\end{aligned} \tag{4.6}$$

where ω is $e^{-2\pi j/N}$ from N size DFT and p is the pilot period. The $\mathbf{\Omega}$ matrix elements are well structured that for the element at a certain k-th row and l-th column can be obtained as

$$\Omega(k,l) = \omega^{(pkl)}. \tag{4.7}$$

Since the elements in $\mathbf{\Omega}$ are exponent function, any matrix element can be obtained with multiplication of two others elements as

$$\Omega(k_1 + k_2, l) = \Omega(k_1, l) \times \Omega(k_2, l) = \omega^{(k_1 pl)}\omega^{(k_2 pl)}. \tag{4.8}$$

Furthermore, the sensing matrix also still has the periodicity and symmetry properties from the DFT matrix. The k and l from eq. 4.7 define the degree of the ω. Because the degree has a modulo of 2π property, there will exist a periodicity of the same element at several rows of the sensing matrix. We can express the each element in Eq. 4.7 as

$$\begin{aligned}\Omega(k,l) &= e^{jmod(\frac{(2\pi pkl)}{N}, 2\pi)} \\ &= e^{2\pi jmod(\frac{(pkl)}{N}, 1)},\end{aligned} \tag{4.9}$$

where $mod(a, b)$ defines the modulo operation of dividend a and divisor b. It easy to conclude from Eq. 4.9 that for k-th row index, where k is a big common divisor

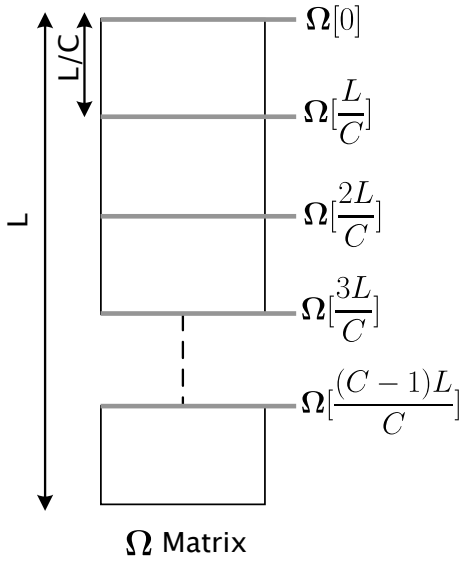

Figure 4.2: C unique rows in $\mathbf{\Omega}$ matrix

of N, there will exist a periodicity of the same elements at that row. Because, N is a multiples of 2 number, we can find big divisors of N in L by dividing L with C evenly, where C is also a multiples of 2 number as shown in Fig. 4.2.

Using Eq. 4.8 and Eq. 4.9, we can compute C rows of the sensing matrix at once in relation to the C unique rows which shown in Fig. 4.2 as

$$\begin{bmatrix} g_{[k]} \\ g_{[k+L/C]} \\ g_{[k+2L/C]} \\ \vdots \\ g_{[k+L(C-1))/C]} \end{bmatrix} = \mathbf{\Gamma} diag(\boldsymbol{\psi}_0[k])\mathbf{r}, \tag{4.10}$$

where matrix $\mathbf{\Gamma} \in \mathbb{C}^{C\times T}$ consists all of the C unique rows in the sensing matrix $\mathbf{\Omega}$ as

$$\mathbf{\Gamma} = \left[\mathbf{\Omega}[0]\, \mathbf{\Omega}[\tfrac{L}{C}]\, \mathbf{\Omega}[\tfrac{2L}{C}]\, \ldots \mathbf{\Omega}[\tfrac{(C-1)}{C}]\right]^T. \tag{4.11}$$

The main idea is to further reduce the complexity by sharing the multiplier for the same matrix coefficients at the same row. To find the number of different elements at each k-th row, we can reduce the constant fraction $(pk)/N$ to its lowest term

using greatest common divisor (GCD). The number of unique coefficient at a k-th row can be defined as

$$U_r = \frac{N}{GCD(pk, N)} \tag{4.12}$$

Then the total of unique multiplier in the matrix $\mathbf{\Gamma}$ is as follow

$$U = \sum_{i=1}^{C-1} \frac{N}{GCD(ipL/C, N)}. \tag{4.13}$$

Moreover, there is a symmetry property in the matrix $\mathbf{\Gamma}$. Because the elements of $\mathbf{\Gamma}$ matrix can be represented using complex unit circle and these elements will divide this complex unit circle evenly. Thus, by using only the elements on the first quadrant of complex unit circle (phase less than $\pi/2$), we can obtain all the different elements located on other quadrants. In term of quadrants, the elements of $\mathbf{\Gamma}$ matrix can be defined as

$$\mathbf{\Gamma}_{(k,l)} = \begin{cases} \mathbf{\Gamma}_{q1(\theta_{k,l})} = e^{-j\theta_{k,l}}, & 0 < \theta_{k,l} \leq \frac{\pi}{2} \\ \mathbf{\Gamma}_{q2(\theta_{k,l})} = -j\mathbf{\Gamma}_{q1(mod(\theta_{k,l}, \frac{\pi}{2}))}, & \frac{\pi}{2} < \theta_{k,l} \leq \pi \\ \mathbf{\Gamma}_{q3(\theta_{k,l})} = -\mathbf{\Gamma}_{q1(mod(\theta_{k,l}, \frac{\pi}{2}))}, & \pi < \theta_{k,l} \leq \frac{3\pi}{2} \\ \mathbf{\Gamma}_{q4(\theta_{k,l})} = j\mathbf{\Gamma}_{q1(mod(\theta_{k,l}, \frac{\pi}{2}))}. & \frac{3\pi}{2} < \theta_{k,l} \leq 2\pi \end{cases} \tag{4.14}$$

The multiplications with -1, j and $-j$ are needed to recover all the elements in other quadrants. However, the multiplication with -1, j and $-j$ can be considered to be negligible compare to a full complex multiplication. By exploiting this property, the Eq. 4.13 can be redefined as

$$U = \sum_{i=1}^{C-1} \left\lceil \frac{N}{4GCD(ipL/C, N)} \right\rceil. \tag{4.15}$$

The matrix strength reduction is done by decomposing matrix $\mathbf{\Gamma}$ into three components as

$$\mathbf{\Gamma} = \mathbf{\Gamma}_3\mathbf{\Gamma}_2\mathbf{\Gamma}_1. \tag{4.16}$$

The first component $\mathbf{\Gamma}_1$ is a matrix which only consist of 1, $-j$, -1 and j component. This matrix creates the quadrant symmetry property as shown in Eq.

4.14. The structure of $\mathbf{\Gamma}_1 \in \mathbb{C}^{U \times T}$ matrix is defined as

$$\mathbf{\Gamma}_1 = \begin{bmatrix} 1 & 1 & 1 & 1 & 1 & \cdots & 1 \\ 1 & 0 & -j & 0 & -1 & \cdots & 0 \\ 0 & 1 & 0 & -j & 0 & \cdots & j \\ & & & \vdots & & & \\ 0 & j & 0 & -1 & 0 & \cdots & 1 \end{bmatrix}. \tag{4.17}$$

Then we can multiply the output from $\mathbf{\Gamma}_1$ with the U unique coefficients, which represented by $\mathbf{\Gamma}_2 \in \mathbb{C}^{U \times U}$ matrix as

$$\mathbf{\Gamma}_2 = \begin{bmatrix} e^{\frac{-j2\pi}{N}} & 0 & 0 & 0 & 0 \\ 0 & e^{\frac{-j4\pi}{N}} & 0 & 0 & 0 \\ 0 & 0 & e^{\frac{-j6\pi}{N}} & 0 & 0 \\ 0 & 0 & 0 & \ddots & 0 \\ 0 & 0 & 0 & 0 & e^{\frac{-j\pi}{2}} \end{bmatrix}. \tag{4.18}$$

The diagonal of $\mathbf{\Gamma_2}$ matrix is filled with U different elements in $\mathbf{\Gamma}$ matrix, which values in range of $e^{\frac{-j2\pi}{N}}$ to $e^{\frac{-j\pi}{2}}$. The last step is to sum the output from $\mathbf{\Gamma}_2$ that corresponds to the same row at the original $\mathbf{\Gamma}$ matrix. This operation can be described by the $\mathbf{\Gamma}_3 \in \mathbb{C}^{C \times U}$ matrix as

$$\mathbf{\Gamma}_3 = \begin{bmatrix} 1 & 1 & 0 & 0 & 0 & \cdots & 0 \\ 0 & 0 & 1 & 1 & 0 & \cdots & 0 \\ 0 & 0 & 0 & 0 & 1 & \cdots & 0 \\ & & & \vdots & & & \\ 0 & 0 & 0 & 0 & 0 & \cdots & 1 \end{bmatrix}. \tag{4.19}$$

Here only the multiplication with matrix $\mathbf{\Gamma_2}$ matrix requires a full complex number multipliers.

Finally the total rnumber of multipliers required to compute the inner product of $\mathbf{\Omega}$ matrix is

$$U_{tot} = (T + U)\frac{L}{C} \tag{4.20}$$

We also can consider this method as a column reduction where the strength reduction technique decrease the column from L into Q as shown in Fig. 4.1.

Where Q is defined as

$$Q = \frac{L}{C} + \frac{U}{T}. \tag{4.21}$$

4.3 Observation Vector Optimization

There are several criterion to define the number of observation vector needed in the CS computation. The most common one is the restricted isometric property (RIP). RIP shows that a matrix behaves as a orthonormal matrix when dealing with sparse signal. For a channel estimation problem as shown in the Eq. (3.10), the sensing matrix ($\mathbf{\Psi}$) is RIP if there exist a constant $\delta\,(0 < \delta < 1)$ for all sparse vector ($\mathbf{a}$) which satisfy below equation as

$$1 - \delta||\mathbf{a}||_2^2 \leq ||\mathbf{\Psi a}||_2^2 \leq (1+\delta)||\mathbf{a}||_2^2. \tag{4.22}$$

If the sensing matrix has the RIP, the minimum number of observation vector required for the CS computation is 2κ, where κ is the sparsity level. However, in the channel estimation problem an RIP matrix only can achieved when utilizing random position pilot [66].

Mutual incoherence property (MIP) is another most used criterion for the CS computation. Different with the RIP, every matrix will have a certain level of MIP. The MIP level of matrix $\mathbf{A}$ is defined as

$$\mu(\mathbf{A}) = \max_{1 \leq l,k \leq M, l \neq k} \frac{|\mathbf{a}_l^T \mathbf{a}_k|}{||\mathbf{a}_l||_2 . |\mathbf{a}_k||_2}, \tag{4.23}$$

where $\mathbf{a}_l$ is the l-th column of matrix $\mathbf{A}$. The mutual coherence will define the maximum sparse element matrix $\mathbf{A}$ can recover

$$\kappa_{max} = \left\lfloor \frac{1}{2}\left(\frac{1}{\mu(\mathbf{A})} + 1\right)\right\rfloor. \tag{4.24}$$

From Eq. (4.23) also we can specify the maximum MIP level to recover a certain signal with sparsity κ_{max} as

$$\mu_{max} = \frac{1}{2\kappa_{max} - 1}. \tag{4.25}$$

It can be seen here that the MIP level is inversely proportional to the κ_{max}.

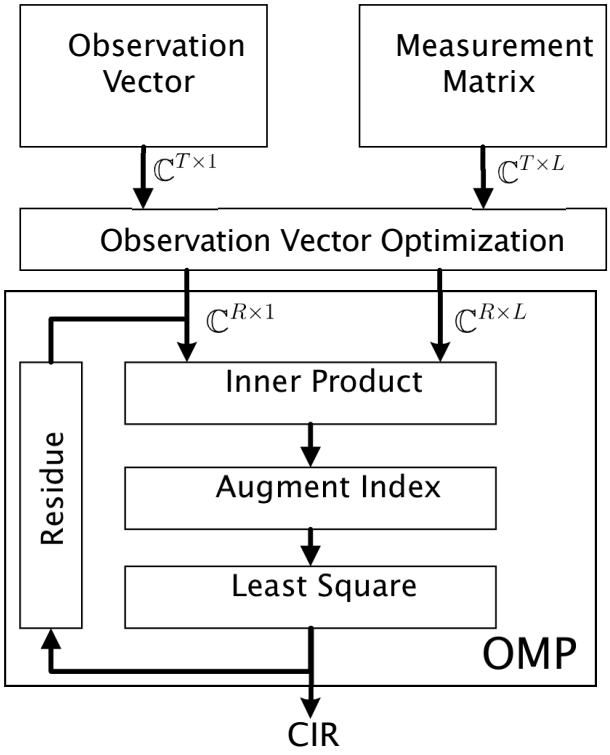

Figure 4.3: Observation vector selection block diagram.

In the CS based channel estimation, basically when reducing the number of pilot will also make the MIP level become higher. We can reduce the number of observation vector until the μ_{max} is reached. In this paper we propose a sensing matrix optimization method by selecting a reduced number of observation vector at the receiver side. The block digram of the proposed method is shown in Fig. 4.3 above. In this proposal, changing the overall system standard is not necessary as the observation vector reduction only exist in the CS computation.

Aliasing will occur when maintaining the same spacing in the observation vector selection [35]. Hence, we propose a observation vector selection with genetic algorithm [56, 67]. Genetic algorithm (GA) is the optimization method that imitate the natural selection [68]. The observation vector chosen by GA will have a non-uniform spacing to each others, so we can avoid the aliasing. The detail of GA which we used in this paper is presented in the Alg. 5. Each R combination from a T set observation vector is treated as an individual. The observation

Algorithm 5 Genetic Algorithm for Pilot Selection

Inputs:

1) Full observation vector number T;
2) Reduce observation vector number R;
3) Crossover probability p_c;
4) Mutation probability p_m;
5) Number of individual in each generation n_d;
6) Number of generation n_g;
7) Discrete probability distribution Ω;

Process:

Create n_d random combination from T observation vector into R subset.
while stopping criterion not met **do**
  Calculate the fitness value of each individual.
  Distribute the selection probability with Ω distribution based on the fitness value.
  for each pair of individual 1 to $n_d/2$ **do**
   Select two individuals based on selection probability.
   For each different chromosome, exchange chromosome with p_c probability.
   For each chromosome in an individual, perform mutation with p_m probability.
   Get two new individuals as part of the next generation.
  end for
  Obtain new generation.
end while
Obtain the best fitness value in the new generation.

location in this R sub-set is considered as a chromosome. Each generation will contain n_d number of individuals. While, the first generation is created with a brute force of a R random combination from T observation vector set.

In each generation, we will calculate the MIP level for each individual which determine the fitness value. Then, we sort these individuals according to its fitness value. In order to create the next generation, the two individual is created by chromosome crossover and mutation of a pair individual in the previous generation. we choose a pair of individuals according to the chosen selection probability Ω. For each pair, we try to exchange the chromosome with the probability p_c. Furthermore, for each chromosome in an individual we try to do a mutation with a probability p_m. The mutation will exchange the current observation in the subset, with a observation outside the pair composite. The mutation probability will be very small compare to the crossover probability. The process of GA will end after a n_g generation have been created, moreover the simulation also will stop if the new generation already become similar to its previous. The fittest individual at the latest generation will be chosen as the final result.

4.4 Simulation Results

To assess the effectiveness of the proposed methods, the ESPAR-OFDM system is simulated with a MATLAB simulation. The quality is measured by using bit error rate (BER) performance and number of multipliers. The simulation use OFDM with 3 elements ESPAR antenna. The ITU-6 typical urban channel is chosen as the channel model in the simulation. Because there will be 3 antenna elements, the channel estimation needs to recover 18 channel impulses. The FFT size is equal to 2048 and the CP length is 1/8 of the OFDM symbol. Correspondingly, the sensing matrix will have a size of 128×768. The simulation parameters are shown in the Table. 4.1.

4.4.1 BER Performance

The first simulation is to show the comparison between SISO-OFDM and OFDM system with 3 elements ESPAR antenna is shown in Fig. 4.4. In this simulation we used the OFDM with QPSK modulation. It can be seen that ESPAR antenna

Table 4.1: Simulation Parameters

Modulation	OFDM with QPSK or 16 QAM
Channel model	ITU 6 Typical Urban
FFT size	2048
Guard interval	1/8 or 1/16 of the OFDM symbol
Equalization	MMSE-SQRD
Pilot	128 Subcarriers with 16 spacing
Data	1920 Subcarriers
Noise	AWGN
Bandwidth	5.575 MHz
ESPAR Antenna	3 Elements
Observation vector optimization	50%

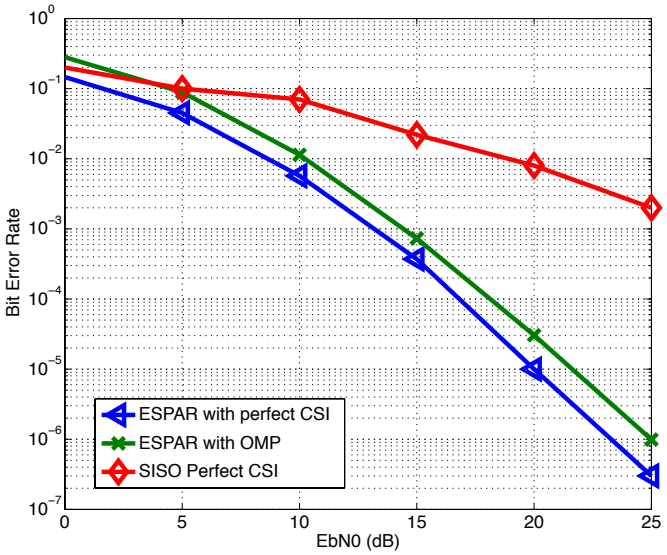

Figure 4.4: SISO OFDM - ESPAR OFDM BER Performance

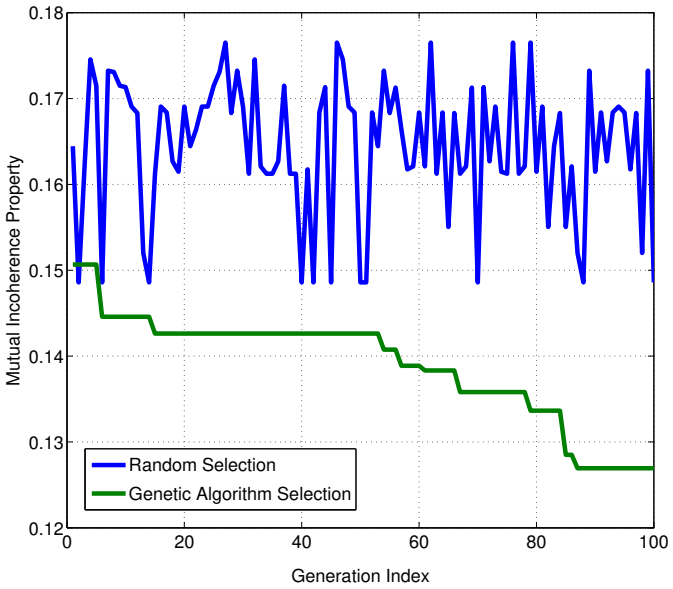

Figure 4.5: MIP Convergent property of the proposed GA pilot selection

can obtain significantly better BER performance compare to the SISO-OFDM system. In this figure, we also include the simulation of the ESPAR-OFDM system with a CS based channel estimation. The performance of the CS based channel estimation only has 1 dB different compared to this ESPAR-OFDM simulation with perfect CSI.

Before we can apply the observation vector optimization method, we need to obtain a set of the observation vector index that correspond to the lowest MIP level. While, the number of possible combination when reducing the vector from 128 to 64 is in order of 10^{37}, thus a brute force random search might not give an optimum solution for this problem. The GA algorithm which is presented in the section 4.3 can provide a sub-optimum solution for selecting the observation vector. In this paper, we run the GA with the total 100 generation n_g, where each generation contains of 100 individual n_d. In each generation we select n_d pairs of individual to create the new generation. Each pair will interchange its chromosome with the posibility of crossover p_c equal to 0.5. While the mutation is performed with much less probability which equal to 0.005. The GA method can obtain the convergence of MIP level compared to the random brute force method

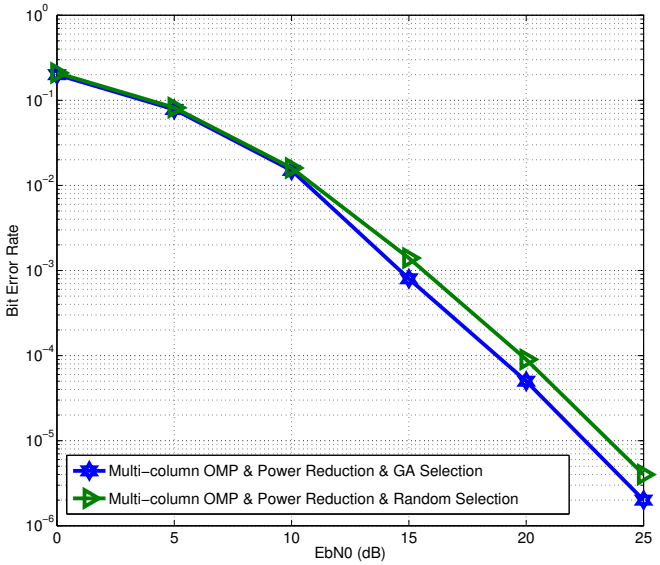

Figure 4.6: BER performance comparison between GA and random method

as shown in Fig. 4.5. Here we can improve the MIP level from 0.153 to 0.126. We also compare the BER performance of the GA and random method for the observation vector optimization in the Fig. 4.6. Here it can be seen that for high Eb/N0 condition ($> 12d$B), the random method will get worse BER performance up to 1 dB.

Finally, we can compare the performance of the 4 approaches in the Fig. 4.7 for QPSK and Fig. 4.8 for 16-QAM modulation. In these figures, it can be seen that the multi-column OMP and the DFT matrix strength reduction have almost the same performance compare to the conventional OMP. The proposed pilot selection technique has a slight 1 dB performance different at high Eb/N0 condition more than 20dB for QPSK. However, almost the same BER performance can be obtained in the system with QAM modulation. The implementation of the observation vector optimization method can bring 30% complexity reduction compared to the approach with multi-column OMP and DFT strength reduction only. This method is useful in the implementation where hardware's area become an important aspect. Furthermore, the computation for the observation vector optimization is done off-line as a pre-computation.

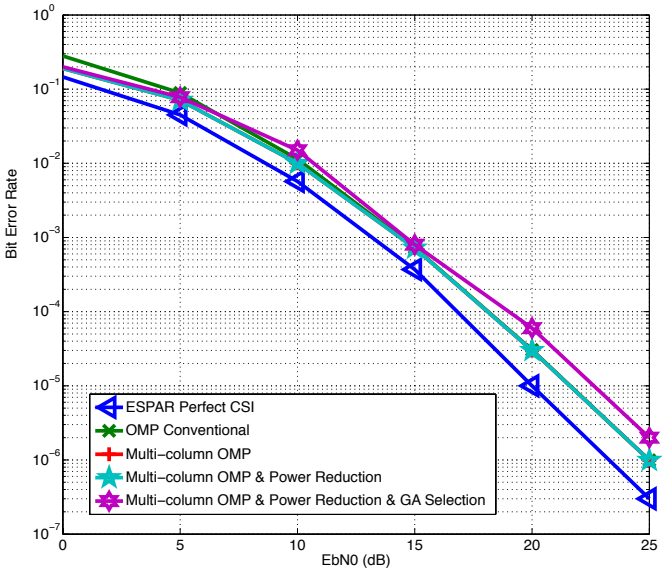

Figure 4.7: Proposed methods BER performance with QPSK modulation

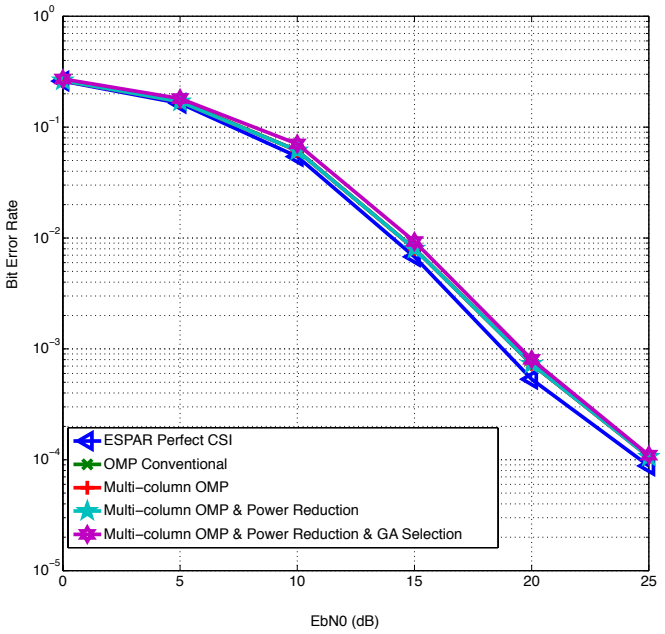

Figure 4.8: Proposed methods BER performance with QAM modulation

4.4.2 Complexity Reduction

The computational requirement for each step of the channel estimation step from Alg. 4 is shown in the Table 4.2. In this table A_n represent the number of the antenna element. At this table, we only include multiplication, division, and coordinate rotation digital computer (CORDIC). Here, the adder and subtractor are considered to be negligible. There are some steps that not require any of these resources. Step 3 is an index augmentation for the vector $\mathbf{\Omega}$ which only requires an addition operation and step 4 is an augmentation for the matrix $\mathbf{\Phi}$ which implemented by a memory fetcher. The matrix $(\mathbf{\Phi}^H\mathbf{\Phi})$ in step 6 can be obtained by taking the row and column of the matrix $(\mathbf{\Psi}^H\mathbf{\Psi})$ that correspond to the sparse locations. Thus, we can compute this matrix multiplication as an off-line precomputation and save it into the memory. In this paper, we assume a matrix inversion by QR decomposition with givens rotation technique is used to solve the least squares problem. Here, the given rotations process is done by an array of CORDIC [62]. A CORDIC only consists of a look up table (LUT) and shifters.

We compare 4 approaches to implement the sensing matrix inner product computation. The conventional method, the multi-column OMP, the multi column OMP with DFT strength reduction and the combination of all the propose methods multi-column OMP, strength reduction and observation vector optimization. The propose methods not only affect the inner product part, but also other steps in the OMP computation. The search of maximum value from the step 2 will deal with a shorter vector if we use the multi-column OMP method. The observation vector optimization also will affect the size of the matrix and vector involve in the multiplications at the step 5 and 9.

To show the effectiveness of our proposal, we simulate our system with the simulation parameters are shown in the Table. 4.1. The simulation has a variation of the guard interval length to assess different L parameter in the sensing matrix. The parameter T is 128, L is 256 and R is 64. The inner product complexity for the conventional method is $3TL$ which are $98,304$ and $49,152$ number of multipliers for GI equal to 1/8 and 1/16 respectively. The multi-column OMP will reduce the inner product complexity by 66%, where the total of required multiplier are TL which translated into $32,768$ and $16,384$ number of multipliers

Table 4.2: Estimated Computational Cost for the Proposed OMP per Iteration

No	Term	×	/	CORDIC
1.	$\mathbf{g} = \langle \mathbf{\Psi}_N^H, \mathbf{r} \rangle$			
	Conventional	$A_n TL$	-	-
	method 1	TL	-	-
	method 1 & 2	$(T+U)L/C$	-	-
	method 1, 2 & 3	$(R+U)L/C$	-	-
2.	$\alpha = arg\ max\|\mathbf{g}\|$			
	Conventional	$A_n L$	-	-
	method 1	L	-	-
	method 1 & 2	L	-	-
	method 1, 2 & 3	L	-	-
3.	$\mathbf{\Omega} = [\alpha + iL]$	-	-	-
4.	$\mathbf{\Phi}_t = \mathbf{\Phi}_{t-1} \| \mathbf{\Psi}_{\mathbf{\Omega}}^H$	-	-	-
5.	$\mathbf{b}_t = \mathbf{\Phi}^H b$			
	Conventional	$A_n T$	-	-
	method 1	$A_n T$	-	-
	method 1 & 2	$A_n T$	-	-
	method 1, 2 & 3	$A_n R$	-	-
6.	$\mathbf{S} = \mathbf{\Phi}^H \mathbf{\Phi}$	-	-	-
7.	$\mathbf{S}^{-1} = inv(\mathbf{S})$	-	-	$\frac{(A_n^2\kappa^2 + A_n\kappa)}{2}$
8.	$\mathbf{a} = \mathbf{S}^{-1}\mathbf{b}_t$	$(A_n^2\kappa^2 - A_n\kappa)/2$	$A_n\kappa$	-
9.	$\mathbf{r} = \mathbf{b} - \mathbf{\Phi}_t \mathbf{a}$			
	Conventional	T	-	-
	method 1	T	-	-
	method 1 & 2	T	-	-
	method 1, 2 & 3	R	-	-
	Total			
	Conventional	$A_n TL + A_n L + A_n + T + (A_n^2\kappa^2 - A_n\kappa)/2$	$A_n\kappa$	$\frac{(A_n^2\kappa^2 + A_n\kappa)}{2}$
	method 1	$TL + L + A_n + T + (A_n^2\kappa^2 - A_n\kappa)/2$	$A_n\kappa$	$\frac{(A_n^2\kappa^2 + A_n\kappa)}{2}$
	method 1 & 2	$(T+U)L/C + L + A_n + T + (A_n^2\kappa^2 - A_n\kappa)/2$	$A_n\kappa$	$\frac{(A_n^2\kappa^2 + A_n\kappa)}{2}$
	method 1, 2 & 3	$(R+U)L/C + L + 2A_n + R + (A_n^2\kappa^2 - A_n\kappa)/2$	$A_n\kappa$	$\frac{(A_n^2\kappa^2 + A_n\kappa)}{2}$

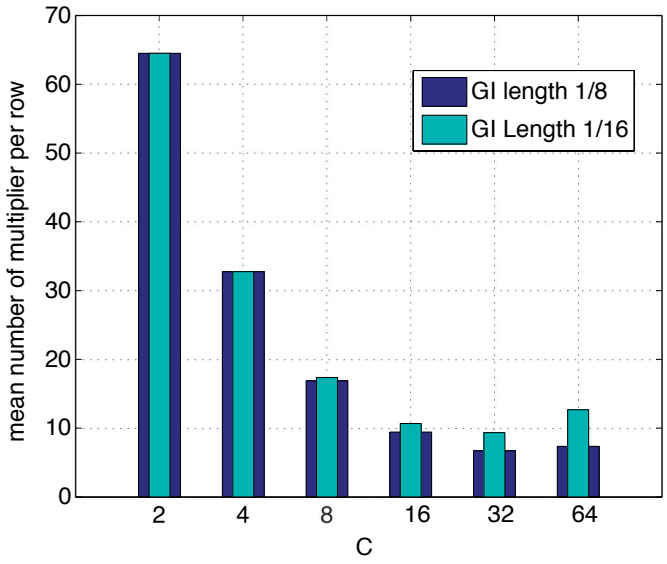

Figure 4.9: Mean number of multipliers per row with different C parameter

for GI equal to 1/8 and 1/16 respectively.

First, we need to find the C parameter which can give a lowest complexity in order to implement the DFT strength reduction. We calculate the mean of the multiplier number per row with different C parameter as shown in the Fig. 4.9. It can be seen in the Fig. 4.9 that with C equal to 32 will correspond to the lowest number of multipliers. Now, using Eq. 4.15 we can find the U parameter to be 87 and 171 for GI equal to 1/8 and 1/16 respectively. Furthermore, the total number of multipliers for the inner product become much lower as 1720 for GI equal to 1/8 and 1196 for GI equal to 1/16. Finally, we can apply the observation vector optimization to reduce the T parameter from 128 into 64.

The comparison of the complexity for the 4 approaches is shown in the Fig. 4.10. By reducing the length of the observation vector into 64, we can gain an additional complexity reduction by 30%. The observation vector optimization method reduces the number of multipliers from $2,897$ into $2,001$ for GI equal to 1/8 and from $2,245$ into $1,518$ for GI equal to 1/16. Finally, we can achieve a total more than 90% of the multiplier reduction using the combination of all the propose methods. For the GI equal to 1/8, we reduce the number of multipliers from $99,993$ into 2001. While for GI equal to 1/16 we reduce the number of

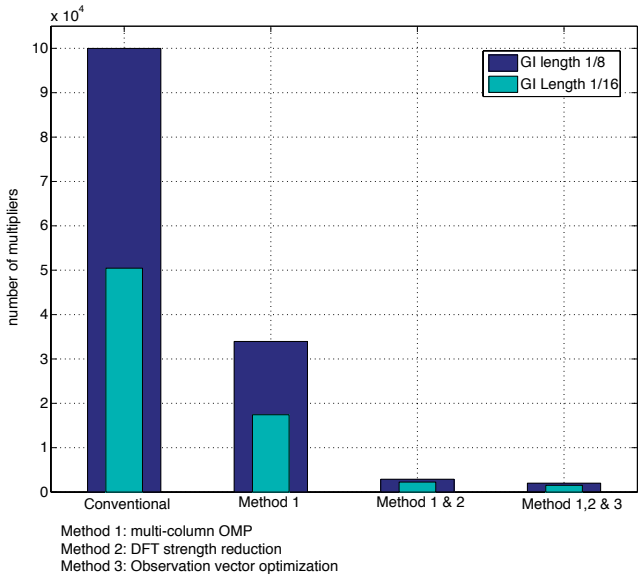

Figure 4.10: Multipliers reduction for inner product computation

multipliers from $50,457$ into $1,158$.

5 Hardware Implementation

This chapter shows the hardware implementation for the proposed low complexity ESPAR-OFDM channel estimation. The hardware design methodology in this dissertation is shown in the Fig. 5.1. The hardware architecture is designed based on the the matlab model of the CS based of the channel estimation for the ESPAR-OFDM system as described in the Chapter 4. The hardware then coded into the Verilog hardware description language (HDL). To assess the hardware, a behavior testbench using Modelsim software is utilized. In this chapter, the first part shows the VLSI architecture of the proposed methods. At the second part we provide a RAM optimization method by exploiting the DFT properties. The third part provides the simulation result for fixed point model to find the minimum bit requirement for the proposed hardware. The last part is the synthesis results for the FPGA implementation.

5.1 VLSI Architecture

In order to simplify the problem, we first created the hardware of CS based channel estimation for conventional SISO OFDM. The hardware for SISO-OFDM will become a base for the channel estimator for OFDM with 3-element ESPAR antenna. Because of the modified 3-column OMP technique, the same inner product and least square modules can be kept for the ESPAR-OFDM implementation. The hardware for ESPAR-OFDM will have a bigger CORDIC array as the length of the CIR become 3 times longer.

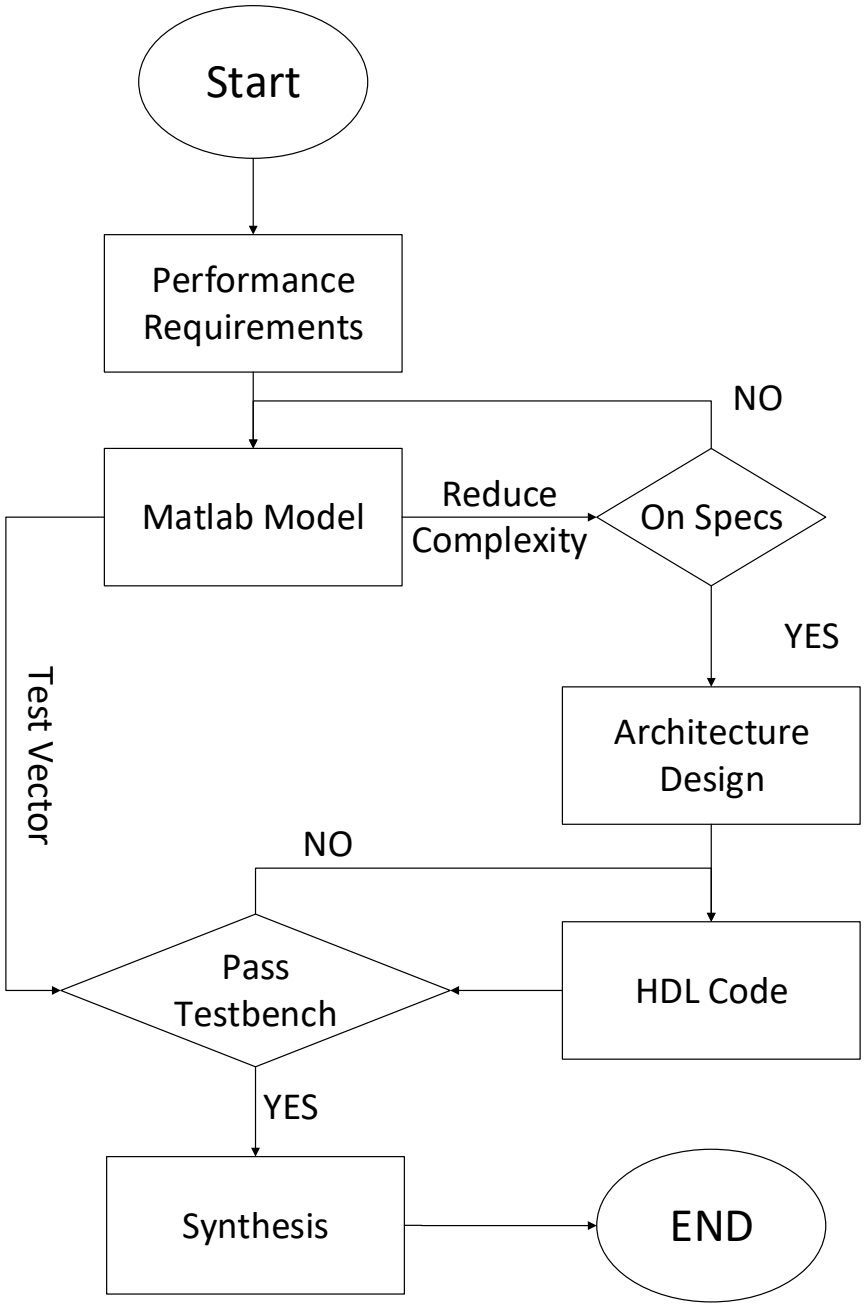

Figure 5.1: Hardware implementation design processes

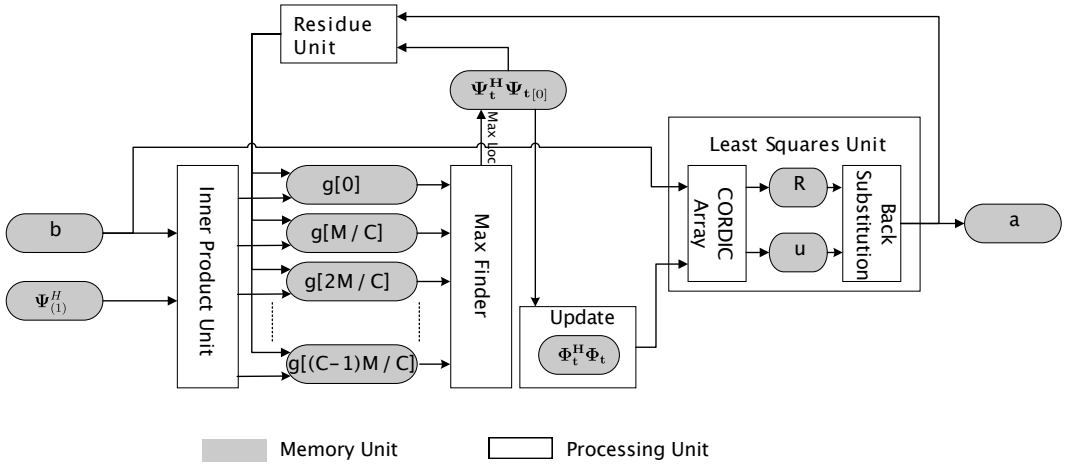

Figure 5.2: Hardware block diagram for CS-based SISO-OFDM channel estimation

5.1.1 CS Based Channel Estimator for SISO OFDM System

There are two considerations in this proposed implementation, a fast execution time to meet the real-time strict deadline and a low resource hardware to support the mobility in ISDB-T one-seg service. Fig.5.2 shows the block diagram for the proposed VLSI architecture. The hardware mainly consists of five processing elements: inner product, maximum finder, $\mathbf{\Phi}^H\mathbf{\Phi}$ matrix updater, least squares and residue unit.

Table 5.1 shows the theoretical memory usage in this hardware implementation. In this table, κ defines the sparsity in the channel impulse response, where $\kappa << N < M$. We save the static variables in the dedicated block RAM (BRAM). While the dynamic variables are saved in the registers, so it can be updated in parallel. By utilizing the proposed memory reduction technique, we can avoid to save the whole complex $\mathbf{\Psi}$ matrix which can significantly reduces the RAM usage.

The least squares operation is realized in two steps as shown in the Fig. 5.4. The first step is the QR decomposition using the givens rotations technique as described in algorithm 2. This operation is done by the systolic array of CORDIC as proposed in the [1]. The structure of the CORDIC array for the QR decom-

Table 5.1: Theoretical memory requirement for CS based channel estimation of SISO-OFDM system

Element	$\mathbf{b}$	$\mathbf{a}$	$\mathbf{g}$	$\mathbf{u}$	$\mathbf{R}$	$\mathbf{\Psi}_{(1)}$	$\mathbf{\Psi}^H\mathbf{\Psi}_{(0)}$	$\mathbf{\Phi}^H\mathbf{\Phi}$
Type	RAM	RAM	Reg	Reg	Reg	RAM	RAM	Reg
Size	N	κ	M	κ	$\kappa\kappa$	N	N	$\kappa\kappa$

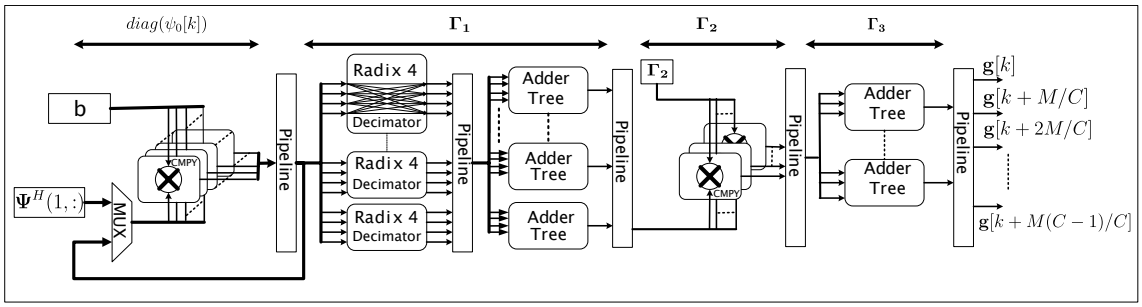

Figure 5.3: Inner product unit for CS-based SISO-OFDM Channel Estimation

position is shown in the Fig. 5.5. Input port x is for the matrix $\mathbf{\Phi}^H\mathbf{\Phi}$, and the input y is for Since $\mathbf{\Psi}^H\mathbf{\Psi}$ is a complex matrix, each processing unit in this systolic array is based on three angles complex rotation (TACR) CORDIC method as proposed in [62]. The outputs from this systolic array are vector $\mathbf{u}$ which is equal to $\mathbf{Q}^H\mathbf{\Phi}^H\mathbf{b}$ and the triangular $\mathbf{R}$ matrix. As the second step, we utilize a back substitution method to get the approximate solution for the channel impulse response $\mathbf{a}$ in each iteration.

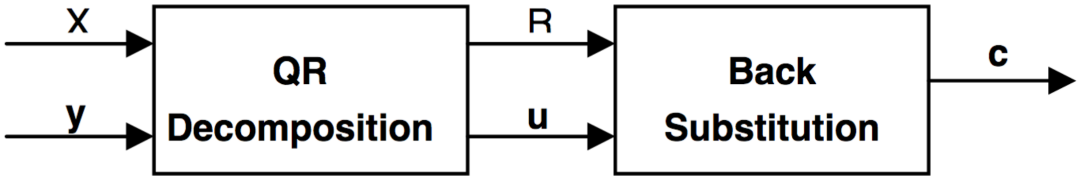

Figure 5.4: Least Square Implementation [1]

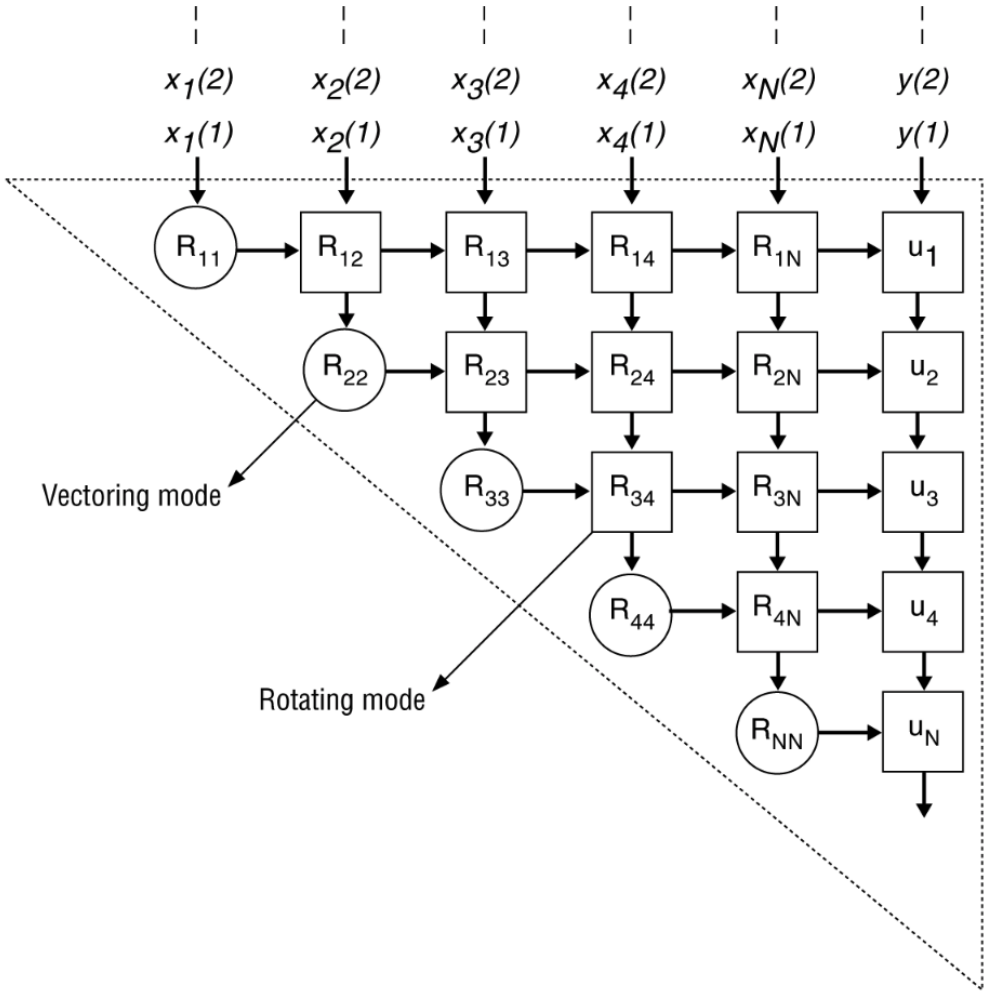

Figure 5.5: CORDIC array structure for the QR decomposition [1]

The details of hardware architecture for the proposed inner product unit is shown in Fig. 5.3. This inner product unit is an iterative realization of the proposed strength reduction method. To compute the inner product $\mathbf{g} = \langle \mathbf{\Psi}^H, \mathbf{r} \rangle$, this module will compute C number of $\mathbf{\Psi}^H$ rows at once in each iteration, thus the whole inner product computation only require M/C clock cycles. This module can be divided into 5 sub-modules. In this implementation, each part is separated by a pipelined register to obtain faster clock speed. In this unit, only the first and the fourth sub-modules that require the complex multiplication. The first sub-module is the realization of $diag(\boldsymbol{\psi}_0[k_1])$ multiplication from Eq. (4.10) which requires N multipliers. While the fourth sub-module uses U number of multipliers as the realization of $\mathbf{\Gamma}_2$ matrix multiplication from Eq. (4.18). The second sub-module is implemented with parallel of radix 4 decimators to realize the multiplication with $\mathbf{\Gamma}_1$ matrix from Eq. (4.17) which only contains 1, j, -1 and $-j$ elements. The third and the fifth sub-modules are implemented with adder threes to perform the summation computation.

5.1.2 CS Based Channel Estimator for OFDM System with 3-Element ESPAR Atenna

The hardware block diagram for the proposed CS based channel estimation for ESPAR-OFDM system is shown in the Fig. 5.6. The difference between the ESPAR version with the SISO version is in the observation vector optimizer, residue unit, and vector $\mathbf{\Theta}$ processor as shown in the Fig. 5.7. Because of the pilot tones in the matrix $\mathbf{P}$ are only consists of BPSK signal which are 1 and -1, the multiplication with this matrix only requires 2's complement negation. Matrix $\mathbf{G}_p$ and matrix $\mathbf{G}_n$ are the shifting matrix in postive and negative direction respectively. Finally, the vector $\mathbf{\Theta}$ can be obtained by a series of three ports adder for every adjacent elements in the $\mathbf{Pr}$ vector. Furthermore, the same inner product module and maximum finder can be used in the ESPAR-OFDM channel estimation.

In the ESPAR-OFDM channel estimation, the least square module need to have a larger CORDIC array to accommodate CIR reconstruction for each antenna element. In each iteration the maximum location from the inner product will be

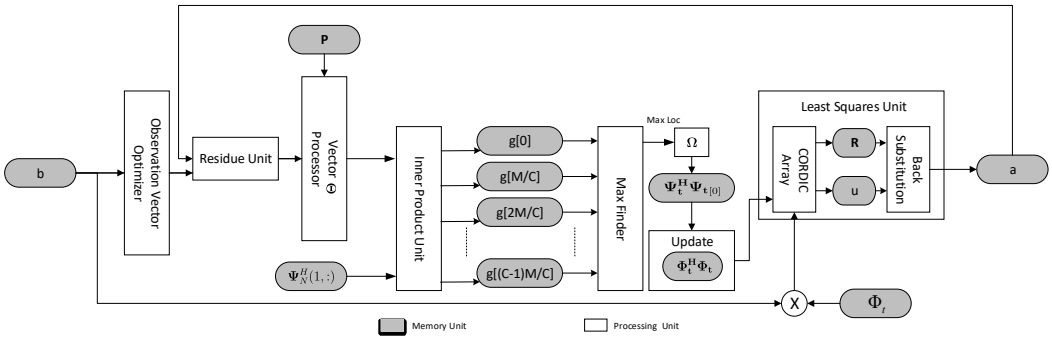

Figure 5.6: hardware Block Diagram for CS-based ESPAR-OFDM Channel Estimation

Table 5.2: Theoretical memory requirement for CS based channel estimation of ESPAR-OFDM system

Element	$\mathbf{b}$	$\mathbf{a}$	$\mathbf{g}$	$\mathbf{u}$	$\mathbf{R}$	$\mathbf{\Psi}_{(1)}$	$\mathbf{\Psi}^H\mathbf{\Psi}_{(0)}$	$\mathbf{\Phi}^H\mathbf{\Phi}$	$\mathbf{\Phi}$	$\mathbf{P}$
Type	RAM	RAM	Reg	Reg	Reg	RAM	RAM	Reg	Reg	Reg
Size	T	κ	L	κ	$\kappa\kappa$	T	T	$\kappa\kappa$	T	T

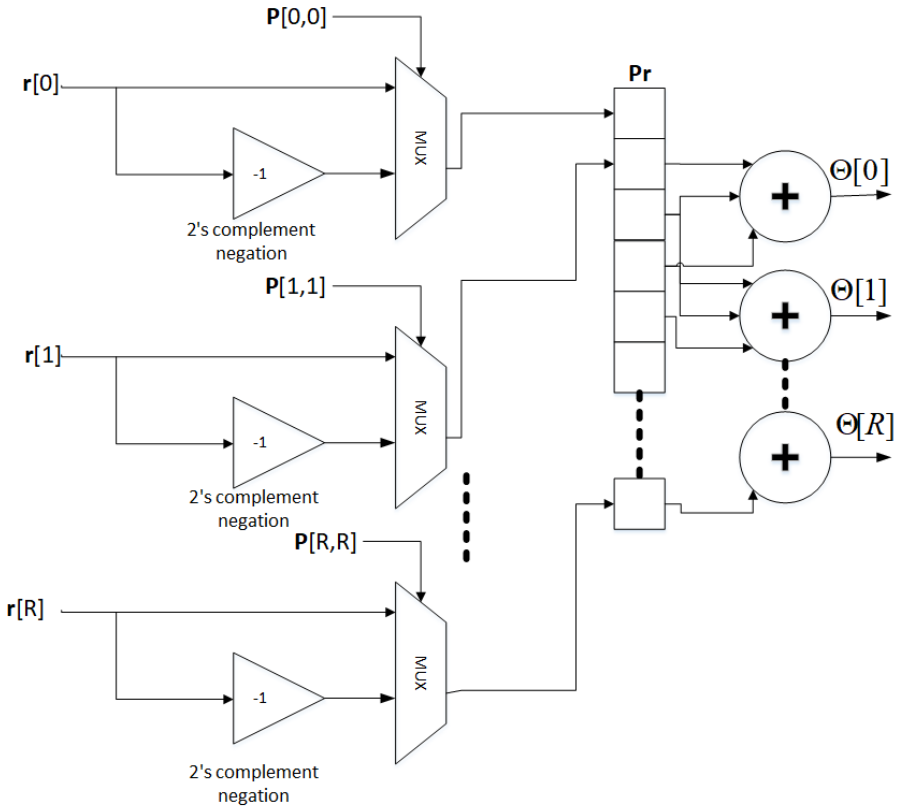

Figure 5.7: VectorΘ processor.

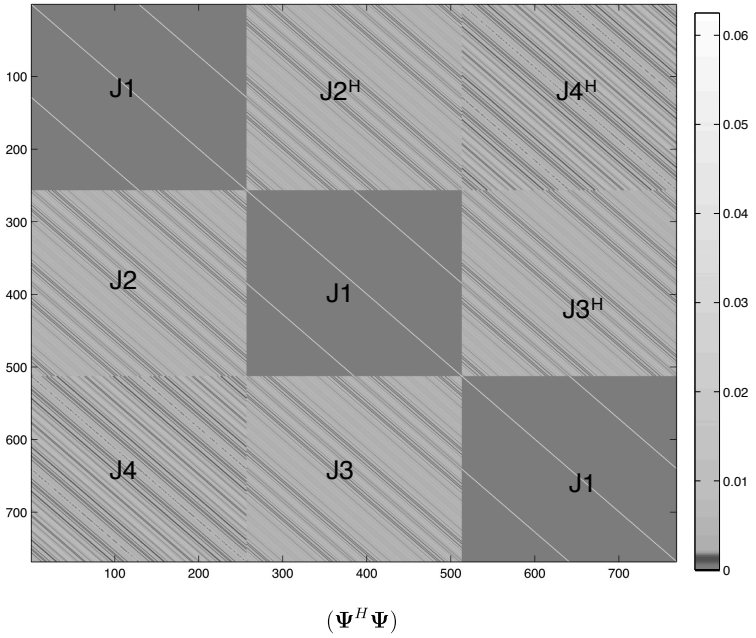

Figure 5.8: matrix $(\mathbf{\Psi}_t^H\mathbf{\Psi}_t)$ structure

used to construct vector $\mathbf{\Omega}$ which has a size of 3. Because of the DFT property, the matrix $(\mathbf{\Phi}_t^H\mathbf{\Phi}_t)$ can be obtained by taking a row and column from matrix $(\mathbf{\Psi}_t^H\mathbf{\Psi}_t)$ that correspond to the sparse location in the vector $\mathbf{\Omega}$. While matrix $(\mathbf{\Psi}_t^H\mathbf{\Psi}_t)$ can be precomputed and save into the RAM. In result, we can avoid the matrix-matrix multiplication with a simple memory fetching.

The matrix $(\mathbf{\Psi}_t^H\mathbf{\Psi}_t)$ has a very large size of $L \times L$ which requires a big size of RAM to store its data. However, because the it is from the DFT matrix the structure of matrix $(\mathbf{\Psi}_t^H\mathbf{\Psi}_t)$ is unique as shown in the Fig. 5.8. We can divide the matrix into 9 sub-matrices where each part has a Toeplitz structure. Moreover, the matrix value can be categorized as 4 matrices $J1$, $J2$, $J3$, and $J4$. The matrix $J1$ will correspond to three sub-matrices, while $J2$, $J3$ and $J4$ each correspond to two pair of a sub-matrix and its conjugate.

By exploiting the Toeplitz and the matrix structure in the Fig. 5.8, we can reduce the RAM requirement by only store 4 array with the length of L, which value are the first column of each matrix $J1$, $J2$, $J3$, and $J4$. A circular shifter is used to obtain the value of others column in the sub-matrix. Finally, we can

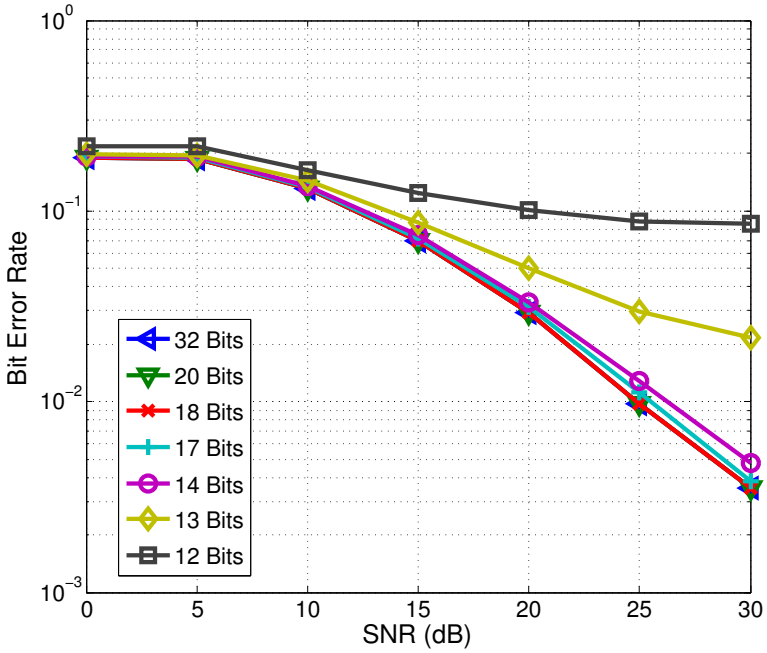

Figure 5.9: Fixed point simulation for SISO-OFDM

reduce the memory requirement to store matrix $(\mathbf{\Psi}_t^H \mathbf{\Psi}_t)$ from $L \times L$ into $4L$.

5.2 Fixed-point Simulation

We also use the MATLAB simulation to find the minimum fixed-point data representation which will not affect our proposed system performance to benefit the hardware implementation. Fig. 5.9 shows the bit error rate performance for this simulation. It can be seen that by reducing the data representation to using 18 bits will not largely affect the BER performance. However, the BER will start to increase if using 17 bits as fixed point for data representation, and the whole system will fail to operate if using 12 bits for data representation.

While the fixed point simulation for the ESPAR-OFDM system using the proposed channel estimation can be seen in the Fig. 5.10 and Fig. 5.11 Here it can be seen that the number of bit can be reduced until 16 bits without a significant changes in the BER performance. Using 14 bit will reduce the performance as much as 3 dB for the low Eb/N0 region. Furthermore, using 12 bit reduce the

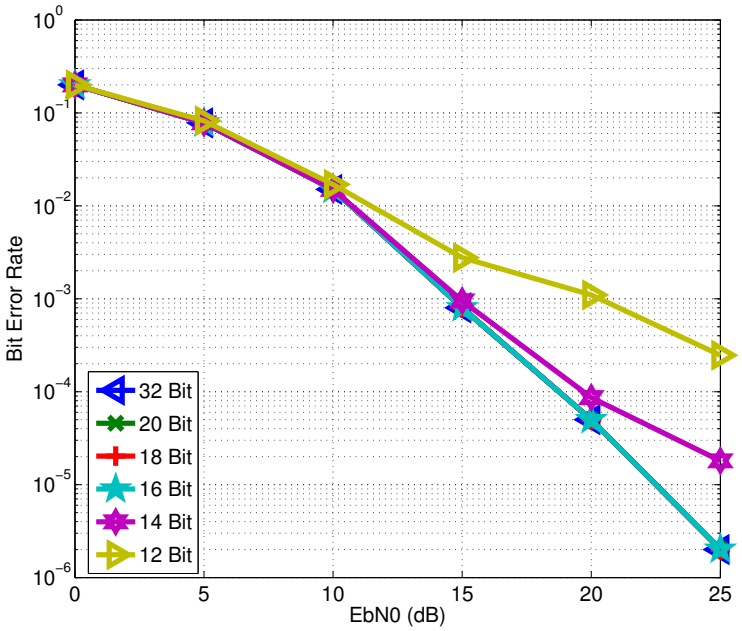

Figure 5.10: Fixed point simulation for ESPAR-OFDM with QPSK modulation

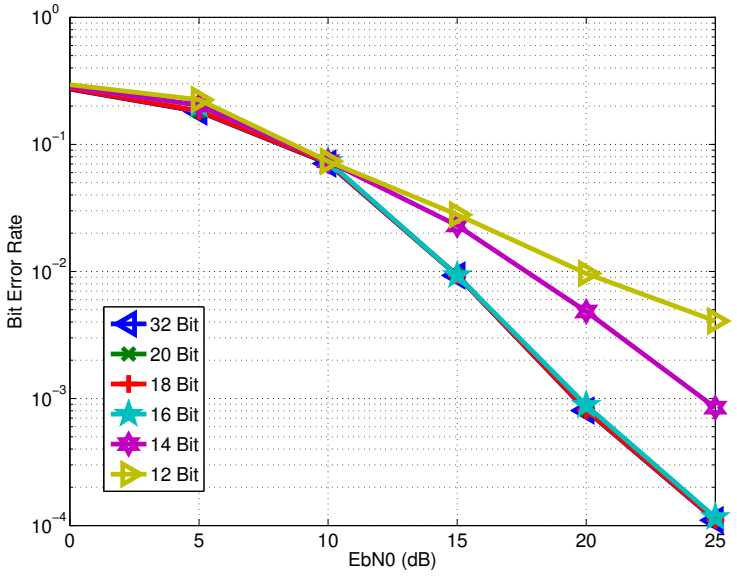

Figure 5.11: Fixed point simulation for ESPAR-OFDM with 16-QAM modulation

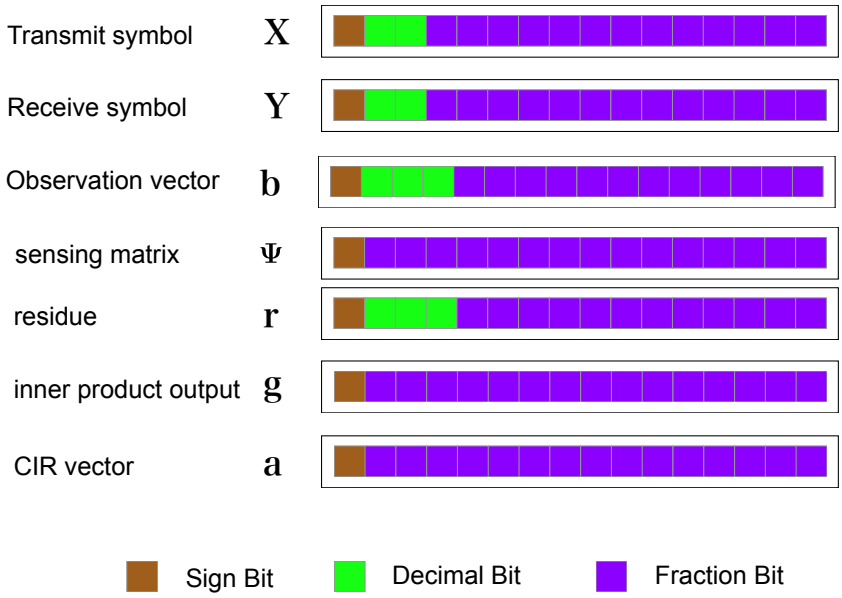

Figure 5.12: Fixed point data representation for each OMP variable

BER performance more than 8 dB at the high Eb/N0 region.

The Matlab simulation is done in the order of 10^6 numbers of OFDM symbol. The minimum and maximum value for each variable can be observed from the Matlab simulation. Thus, we can optimized the fixed-point representation of each variable according to its maximum and minimum value. Fig. 5.12 shows the data representation for each variable used in the hardware and fixed-point simulation. The fixed point data representation here use two's complement format.

5.3 Synthesis Results

The proposed hardware is realized in Verilog HDL and synthesized into Xilinx Virtex 6 FPGA. Based on the MATLAB simulation results, the hardware is realized with specification $C = 32$ and data representation with 16 bits as fixed points. The measurement matrix $\mathbf{\Psi}$ has a dimension of $T = 128$, $R = 64$ and $L = 256$. The sparsity degree of the channel impulse response is $\kappa = 6$.

The synthesis results for the FPGA resources utilization can be seen in table 5.3. Using the proposed method, the hardware can be fit into Xilinx Virtex 6

Table 5.3: FPGA Xilinx Virtex 6 Resource Utilization

Max Frequency	100 MHz
Occupied Slices	24,720 (11.67%)
DSP48 Cores	299(14.7%)
BRAM	61.4kb (1.6%)
Register	184 kb (31 %)

XC6VSX475T. The proposed architecture only require 1.6 % BRAM and 31% register utilization. Moreover, this design is operated with 100 MHz clock speed.

The inner product multiplication execution time requirement can be calculated as

$$T_{ip} = (\frac{M}{C} + 5) \times T_{clock}. \tag{5.1}$$

Since $C = 32$ and $M = 256$, the M/C will be equal to 8, thus, it will require 13 clock cycles which is equal to 130 ns. While the least squares execution time can be calculated as

$$T_{ls} = 5\kappa \times T_{clock}. \tag{5.2}$$

The least squares will require 90 clock cycle or 900 ns. The residue vector can be computed in every time a component of vector a can be obtained from the least squares back substitution. The rest of the hardware modules execution time are as follows. The maximum finder requires 8 clock cycle for $M = 256$, the $\mathbf{\Phi}^H\mathbf{\Phi}$ needs κ clock cycle and the residue unit require 18 clock cycle. Therefore, the total reconstruction time can be calculated as

$$T_{tot} = \kappa(T_{ip} + T_{ls} + 26 + \kappa)/3, \tag{5.3}$$

for the sparsity degree as 18, the reconstruction time is $8.82\mu s$. The comparison of the proposed implementation compare to the existing design is shown in the Table. 5.4. It was greatly reduce while the fastest available design requires 158.7 μs.

Peak signal-to-noise ratio (PSNR) is used to assess the hardware reconstruction quality. PSNR show the ratio between the noise created by the hardware and the

Table 5.4: Comparison to existing design

Hardware	Matrix Size	Sparsity	Clock	Process Time	Data Format
Intel Core i7 [69]	64 x 512	12	3 GHz	25ms	single precision real data
NVIDIA GTX480 [70]	512x8192	64	N/A	15ms	N/A
Virtex 6 [28]	256 x 1024	12	100MHz	158.7 μs	18 bit fixed point real data
Virtex 6 [30]	256 x 1024	36	120MHz	350 μs	18 bit fixed point real data
Virtex 7 [31]	512 x 2048	12	165MHz	391 μs	18 bit fixed point real data
Virtex 6 (proposed)	128 x 768	18	100MHz	8.82 μs	16 bit fixed point real data

Table 5.5: Hardware PSNR comparison

Hardware	Virtex 6 [28]	Virtex 6 [30]	Virtex 7 [31]	Proposed
PSNR (dB)	23.5	38.8	N/A	49.7

original signal. PSNR is computed as

$$PSNR = 20log\left(\frac{MAX}{\sqrt{MSE}}\right). \tag{5.4}$$

Where mean square error (MSE) is defined as the mean square difference between the reconstructed signal from OMP hardware and the original signal. MSE is computed as

$$MSE = \frac{1}{L}\sum_{i=0}^{L}\left[x(i) - \hat{x}(i)\right]^2. \tag{5.5}$$

The PSNR comparison between existing design is shown in the Table. 5.5.

6 Conclusion

ESPAR antenna is a promising replacement for the conventional multi-antenna system such as MIMO with lower power consumption and smaller hardware size with only one RF front-end. However, the implementation of the ESPAR antenna in the wireless communication system is hindered by its channel estimation computational cost. This dissertation provided three methods for the computational cost reduction for ESPAR-OFDM channel estimation. Moreover a parallel VLSI architecture is proposed to achieve fast execution time in regards to the wireless system real-time computation deadline.

Chapter 3 introduced the ESPAR antenna structure and its circuit model. Furthermore, this chapter also shows the implementation of the ESPAR antenna to the OFDM system. The ESPAR-OFDM channel characteristics and the available CS based channel estimation were introduced in this chapter.

The main contribution of this dissertation was presented in the Chapter 4. An implementation if the CS based algorithm for the channel estimation in the OFDM system has several unique properties. Three methods were proposed to reduce the CS inner product computational cost. First, the CIR has the same delay profile for each ESPAR antenna elements. By exploiting this property, a new multi-column CS algorithm was introduced. Furthermore, a matrix strength reduction was applied by taking advantage the CS sensing matrix structure which based on the DFT matrix. The third reduction was using the property of the CS algorithm itself which can work with less sampling, here a observation vector optimization method also introduced to gain lower complexity. The combination of the proposed methods can reduce the CS inner product computational cost by 97.7%.

Beside algorithm based computational reduction, this dissertation also provided the hardware implementation for the proposed ESPAR-OFDM channel estima-

tion. The main purpose of the hardware implementation is to achieve a faster execution time to met the wireless system deadline requirement as shown in the Table 1.1. A VLSI architecture with a 32 level of parallelism was proposed in this chapter. The proposed structure can achieve 1700% increment in the execution time which can met any modern OFDM based wireless communication system timing deadline.

References

[1] D. Boppana, K. Dhanoa, and J. Kempa. FPGA based embedded processing architecture for the QRD-RLS algorithm. In *Proceeding of 12th Annual IEEE Symposium on Field-Programmable Custom Computing Machines, 2004. FCCM 2004.*, pages 330–331, April 2004.

[2] M. Schwartz and C. Batchelor. The origins of carrier multiplexing: Major george owen squier and AT&T. *IEEE Communications Magazine*, 46(5):20–24, May 2008.

[3] R. C. Boyd and F. J. Herr. The n2 carrier terminal — objectives and analysis. *Bell System Technical Journal*, 44(5):731–759, 1965.

[4] B. Saltzberg. Performance of an efficient parallel data transmission system. *IEEE Transactions on Communication Technology*, 15(6):805–811, December 1967.

[5] R. Chang and R. Gibby. A theoretical study of performance of an orthogonal multiplexing data transmission scheme. *IEEE Transactions on Communication Technology*, 16(4):529–540, August 1968.

[6] B. Hirosaki. An orthogonally multiplexed QAM system using the discrete fourier transform. *IEEE Transactions on Communications*, 29(7):982–989, July 1981.

[7] S. B. Weinstein. The history of orthogonal frequency-division multiplexing. *IEEE Communications Magazine*, 47(11):26–35, November 2009.

[8] IEEE standard for information technology–telecommunications and information exchange between systems local and metropolitan area networks–specific

requirements part 11: Wireless lan medium access control (MAC) and physical layer (PHY) specifications. *IEEE Std 802.11-2012 (Revision of IEEE Std 802.11-2007)*, pages 1–2793, March 2012.

[9] Long term evolution (LTE3gpp) physical layer, general description. *3GPP TS36.201 Release 8*, 2008.

[10] Transmission system for digital terrestrial television broadcasting. *ARIB STD-B31 Revision 1.6*, 2005.

[11] O. Besson and P. Stoica. On parameter estimation of MIMO flat-fading channels with frequency offsets. *IEEE Transactions on Signal Processing*, 51(3):602–613, March 2003.

[12] Lizhong Zheng and D. N. C. Tse. Diversity and multiplexing: a fundamental tradeoff in multiple-antenna channels. *IEEE Transactions on Information Theory*, 49(5):1073–1096, May 2003.

[13] R. Schlub, Junwei Lu, and T. Ohira. Seven-element ground skirt monopole ESPAR antenna design from a genetic algorithm and the finite element method. *IEEE Transactions on Antennas and Propagation*, 51(11):3033–3039, Nov 2003.

[14] H. Kawakami and T. Ohira. Electrically steerable passive array radiator (ESPAR) antennas. *IEEE Antennas and Propagation Magazine*, 47(2):43–50, April 2005.

[15] H. Cox, R. Zeskind, and M. Owen. Robust adaptive beamforming. *IEEE Transactions on Acoustics, Speech, and Signal Processing*, 35(10):1365–1376, Oct 1987.

[16] K. L. Bell, Y. Ephraim, and H. L. Van Trees. A bayesian approach to robust adaptive beamforming. *IEEE Transactions on Signal Processing*, 48(2):386–398, Feb 2000.

[17] S. A. Vorobyov, A. B. Gershman, and Zhi-Quan Luo. Robust adaptive beamforming using worst-case performance optimization: a solution to the signal

mismatch problem. *IEEE Transactions on Signal Processing*, 51(2):313–324, Feb 2003.

[18] S. Hara, S. Hane, and Y. Hara. Simple -steering OFDM adaptive array antenna for doppler-shifted signal suppression. *IEEE Transactions on Vehicular Technology*, 54(1):91–99, Jan 2005.

[19] Satoshi Tsukamoto and Minoru Okada. Single-rf diversity receiver for OFDM system using ESPAR antenna with alternate direction. *ECTI Transactions on Computer and Information Technology*, 6(1):89–93, 2012.

[20] D. J. Reinoso Chisaguano and M. Okada. Low complexity submatrix divided MMSE Sparse-SQRD detection for MIMO-OFDM with ESPAR antenna receiver. *VLSI Design*, 2013(Article ID 206909), 2013.

[21] G. G. Raleigh and J. M. Cioffi. Spatio-temporal coding for wireless communication. *IEEE Transactions on Communications*, 46(3):357–366, Mar 1998.

[22] D. J. Reinoso Chisaguano, Y. Hou, T. Higashino, and M. Okada. Low-complexity channel estimation and detection for mimo-ofdm receiver with ESPAR antenna. *IEEE Transactions on Vehicular Technology*, 65(10):8297–8308, Oct 2016.

[23] Diego Javier Reinoso Chisaguano, Yafei Hou, Takeshi Higashino, and Minoru Okada. ISDB-T diversity receiver using a 4-element ESPAR antenna with periodically alternating directivity. *ITE Transactions on Media Technology and Applications*, 3(4):268–278, 2015.

[24] Rian Ferdian, Yafei Hou, and Minoru Okada. Fast and low-complexity orthogonal matching pursuit based channel estimation in ISDB-T receiver with 3-element ESPAR antenna. In *Broadband Multimedia Systems and Broadcasting (BMSB), 2016 IEEE International Symposium on*, pages 1–4. IEEE, 2016.

[25] D.L. Donoho. Compressed sensing. *Information Theory, IEEE Transactions on*, 52(4):1289–1306, April 2006.

[26] E.J. Candes, J. Romberg, and T. Tao. Robust uncertainty principles: exact signal reconstruction from highly incomplete frequency information. *Information Theory, IEEE Transactions on*, 52(2):489–509, Feb 2006.

[27] A. Septimus and R. Steinberg. Compressive sampling hardware reconstruction. In *Circuits and Systems (ISCAS), Proceedings of 2010 IEEE International Symposium on*, pages 3316–3319, May 2010.

[28] Lin Bai, P. Maechler, M. Muehlberghuber, and H. Kaeslin. High-speed compressed sensing reconstruction on FPGA using OMP and AMP. In *Proceedings of 2012 19th IEEE International Conference on Electronics, Circuits and Systems (ICECS)*, pages 53–56, Dec 2012.

[29] J.L.V.M. Stanislaus and T. Mohsenin. High performance compressive sensing reconstruction hardware with QRD process. In *Proceedings of 2012 IEEE International Symposium on Circuits and Systems (ISCAS)*, pages 29–32, May 2012.

[30] Hassan Rabah, A. Amira, B.K. Mohanty, S. Almaadeed, and P.K. Meher. Fpga implementation of orthogonal matching pursuit for compressive sensing reconstruction. *Very Large Scale Integration (VLSI) Systems, IEEE Transactions on*, 23(10):2209–2220, Oct 2015.

[31] Yinghui Quan, Yachao Li, Xiaoxiao Gao, and Mengdao Xing. FPGA implementation of real-time compressive sensing with partial Fourier dictionary. *International Journal of Antennas and Propagation*, 2016(Article ID 1671687), 2016.

[32] S. Yoshizawa and Y. Miyanaga. Vlsi implementation of high-throughput SISO-OFDM and MIMO-OFDM transceivers. In *2006 International Symposium on Communications and Information Technologies*, pages 483–486, Oct 2006.

[33] R. Ferdian, Y. Hou, and M. Okada. Effective vlsi architecture for compressed sensing based channel estimation in isdb-t system. In *15th International Symposium on Communications and Information Technologies (ISCIT)*, Oct 2015.

[34] R. Ferdian, Y. Hou, and M. Okada. A low-complexity hardware implementation of compressed sensing-based channel estimation for ISDB-T system. *IEEE Transactions on Broadcasting*, PP(99):1–11, 2016.

[35] Rian Ferdian, Ratih H Puspita, Yafei Hou, and Minoru Okada. Low complexity compressed sensing based channel estimation with measurement matrix optimization for ofdm system. *IEICE technical report*, 116(318):17–21, 2016.

[36] L. Greenstein. A multipath fading channel model for terrestrial digital radio systems. *IEEE Transactions on Communications*, 26(8):1247–1250, Aug 1978.

[37] S. Weinstein and P. Ebert. Data transmission by frequency-division multiplexing using the discrete fourier transform. *IEEE Transactions on Communication Technology*, 19(5):628–634, October 1971.

[38] N. Benvenuto and S. Tomasin. On the comparison between OFDM and single carrier modulation with a DFE using a frequency-domain feedforward filter. *IEEE Transactions on Communications*, 50(6):947–955, Jun 2002.

[39] T. L. Marzetta and B. M. Hochwald. Capacity of a mobile multiple-antenna communication link in rayleigh flat fading. *IEEE Transactions on Information Theory*, 45(1):139–157, Jan 1999.

[40] Qinfang Sun, D. C. Cox, H. C. Huang, and A. Lozano. Estimation of continuous flat fading MIMO channels. In *2002 IEEE Wireless Communications and Networking Conference Record. WCNC 2002 (Cat. No.02TH8609)*, volume 1, pages 189–193 vol.1, Mar 2002.

[41] F. Rusek, D. Persson, B. K. Lau, E. G. Larsson, T. L. Marzetta, O. Edfors, and F. Tufvesson. Scaling up MIMO: Opportunities and challenges with very large arrays. *IEEE Signal Processing Magazine*, 30(1):40–60, Jan 2013.

[42] H. Zhang and H. Dai. Fast MIMO transmit antenna selection algorithms: a geometric approach. *IEEE Communications Letters*, 10(11):754–756, November 2006.

[43] L. Zhao, K. Li, K. Zheng, and M. Omair Ahmad. An analysis of the tradeoff between the energy and spectrum efficiencies in an uplink massive MIMO-OFDM system. *IEEE Transactions on Circuits and Systems II: Express Briefs*, 62(3):291–295, March 2015.

[44] J. Lee, J. Y. Lee, and Y. H. Lee. Spatial multiplexing of OFDM signals with QPSK modulation over ESPAR. *IEEE Transactions on Vehicular Technology*, 66(6):4914–4923, June 2017.

[45] A. Ando. Analysis of ESPAR antennas in indoor multi-path environments for wireless ad-hoc network systems. In *2002 IEEE Wireless Communications and Networking Conference Record. WCNC 2002 (Cat. No.02TH8609)*, volume 2, pages 586–591 vol.2, Mar 2002.

[46] Bokuji Komiyama, T. Ohira, and S. Tanaka. Espar antenna: an adaptive antenna for mobile terminals and its application to wireless ad hoc networks, 2004.

[47] D.J.R. Chisaguano, T. Higashino, and M. Okada. Isdb-t receiver with single-rf diversity using a 3-element espar antenna. In *Communications and Information Technologies (ISCIT), 2014 14th International Symposium on*, pages 462–465, Sept 2014.

[48] L. Marantis, K. Maliatsos, and A. Kanatas. ESPAR antenna positioning for truck-to-truck communication links. In *2016 10th European Conference on Antennas and Propagation (EuCAP)*, pages 1–5, April 2016.

[49] A. Kausar, H. Mehrpouyan, M. Sellathurai, R. Qian, and S. Kausar. Energy efficient switched parasitic array antenna for 5G networks and IoT. In *2016 Loughborough Antennas Propagation Conference (LAPC)*, pages 1–5, Nov 2016.

[50] M. R. Islam and M. Ali. A 900 MHz beam steering parasitic antenna array for wearable wireless applications. *IEEE Transactions on Antennas and Propagation*, 61(9):4520–4527, Sept 2013.

[51] Misu Kazuki and Miura Jun. Specific person detection and tracking by a mobile robot using 3D LIDAR and ESPAR antenna. *Intelligent Autonomous Systems 13: Proceedings of the 13th International Conference IAS-13*, pages 705–719, 2016.

[52] K. Misu and J. Miura. Specific person tracking using 3D LIDAR and ESPAR antenna for mobile service robots. *Advanced Robotics*, 29(22):1483–1495, 2015.

[53] Baoguo Yang, K. B. Letaief, R. S. Cheng, and Zhigang Cao. Channel estimation for OFDM transmission in multipath fading channels based on parametric channel modeling. *IEEE Transactions on Communications*, 49(3):467–479, Mar 2001.

[54] S. Coleri, M. Ergen, A. Puri, and A. Bahai. Channel estimation techniques based on pilot arrangement in OFDM systems. *IEEE Transactions on Broadcasting*, 48(3):223–229, Sep 2002.

[55] G. Taubock, F. Hlawatsch, D. Eiwen, and H. Rauhut. Compressive estimation of doubly selective channels in multicarrier systems: Leakage effects and sparsity-enhancing processing. *IEEE Journal of Selected Topics in Signal Processing*, 4(2):255–271, April 2010.

[56] X. Ma, F. Yang, W. Ding, and J. Song. Novel approach to design time-domain training sequence for accurate sparse channel estimation. *IEEE Transactions on Broadcasting*, 62(3):512–520, Sept 2016.

[57] W. Ding, F. Yang, C. Pan, L. Dai, and J. Song. Compressive sensing based channel estimation for OFDM systems under long delay channels. *IEEE Transactions on Broadcasting*, 60(2):313–321, June 2014.

[58] Ziji Ma, Shuaifeng Guo, Hongli Liu, and Minoru Okada. Sliding-MOMP based channel estimation scheme for ISDB-T systems. *Mathematical Problems in Engineering*, 2016(Article ID 4571359), 2016.

[59] K. Hayashi, M. Nagahara, and T. Tanaka. A user's guide to compressed sensing for communications systems. *IEICE Transaction on Communication*, E96-B(3):685–712, 2013.

[60] S.G. Mallat and Z. Zhang. Matching pursuits with time-frequency dictionaries. *Signal Processing, IEEE Transactions on*, 41(12):3397–3415, Dec 1993.

[61] J.A. Tropp and A.C. Gilbert. Signal recovery from random measurements via orthogonal matching pursuit. *Information Theory, IEEE Transactions on*, 53(12):4655–4666, Dec 2007.

[62] A. Maltsev, V. Pestretsov, R. Maslennikov, and A. Khoryaev. Triangular systolic array with reduced latency for QR-decomposition of complex matrices. In *Proceedings of 2006 IEEE International Symposium on Circuits and Systems*, pages 385–388, May 2006.

[63] W. Bajwa, J. Haupt, A. Sayeed, and R. Nowak. Compressed channel sensing: A new approach to estimating sparse multipath channels. *Proceedings of the IEEE*, 98(6):1058–1076, June 2010.

[64] Mahdi Cheraghchi, Venkatesan Guruswami, and Ameya Velingker. Restricted isometry of fourier matrices and list decodability of random linear codes. In *Proceedings of the Twenty-Fourth Annual ACM-SIAM Symposium on Discrete Algorithms*, SODA '13, pages 432–442. SIAM, 2013.

[65] J. A. Tropp. Greed is good: algorithmic results for sparse approximation. *IEEE Transactions on Information Theory*, 50(10):2231–2242, Oct 2004.

[66] C. R. Berger, Z. Wang, J. Huang, and S. Zhou. Application of compressive sensing to sparse channel estimation. *IEEE Communications Magazine*, 48(11):164–174, November 2010.

[67] X. He, R. Song, and W. P. Zhu. Pilot allocation for distributed-compressed-sensing-based sparse channel estimation in MIMO-OFDM systems. *IEEE Transactions on Vehicular Technology*, 65(5):2990–3004, May 2016.

[68] K. F. Man, K. S. Tang, and S. Kwong. Genetic algorithms: concepts and applications [in engineering design]. *IEEE Transactions on Industrial Electronics*, 43(5):519–534, Oct 1996.

[69] Alexandre Borghi, Jérôme Darbon, Sylvain Peyronnet, Tony F. Chan, and Stanley Osher. A simple compressive sensing algorithm for parallel many-core architectures. *Journal of Signal Processing Systems*, 71(1):1–20, 2013.

[70] Y. Fang, L. Chen, J. Wu, and B. Huang. GPU implementation of orthogonal matching pursuit for compressive sensing. In *Proceeding of 2011 IEEE 17th International Conference on Parallel and Distributed Systems (ICPADS)*, pages 1044–1047, Dec 2011.

Index